INTERACTIONS OF THE AQUATED FORMS OF RUTHENIUM(III) ANTICANCER COMPLEXES WITH PROTEIN

5A.1 Introduction

Over the past 25 years, a large number of studies have been carried out in order to clarify the mechanism of action of ruthenium complexes towards biomolecular target. In general, increasing evidences in the literature show that mechanism responsible for anticancer activities of ruthenium complexes are based on their DNA nucleobases interaction.[1-3] But before such interaction occurs, these complexes should be passed from cellular membrane to the nuclear membrane. During this time, ruthenium complexes may interact with many active sites such as proteins, peptides and other molecular targets.[4-6] It is well recognized that ruthenium complexes interact with protein receptor immediately after its intravenous administration.[7,8] Transferrin, which is mainly responsible for transporting iron to the body cells could be employed as a natural carrier for delivering cytotoxic ruthenium agents to tumor cells because of their higher demand for iron.[9,10] On the other hand, albumin, a most abundant human plasma protein displays high binding affinity[11] and act as a reservoir for the transferrin cycle. Lots of efforts have been devoted for investigating the interactions between ruthenium complexes and proteins. It is believed that ruthenium complexes tend to coordinate N-side chains of amino acids like histidine, arginine as well as other amino acids, since these complexes are known to bind selectively to imine sites in biomolecules.[12,13] Also there are evidences for binding of ruthenium to sulfur (S donor/thiolate) compounds, but these complexes are kinetically unstable, especially in the presence of oxygen.[14,15] The interactions are generally facilitated by aqua derivatives of ruthenium(III) complexes because these derivatives are much more reactive towards intracellular target as compared to their parent chloro complexes. In case of NAMI-A, very interesting information have been obtained when crystal structures of lactoferrin—NAMI-A[16] and carbonic anhydrase—NAMI-A adducts[17] are examined. The crystal structure of carbonic anhydrase—NAMI-A adduct reveals that ligands of ruthenium complex are progressively lost during protein binding and in final adduct ruthenium complex retains its octahedral arrangement completed by water molecules, imidazolium nitrogen atom of His64 and carbonyl oxygen atom of Asn62 .[17] Recently, Vergara *et. al.*[18] has investigated the binding properties of a new

NAMI-A analogue called azi-Ru, which is more cytotoxic and shows higher antiproliferative activity than NAMI-A towards hen egg lysozyme (HEWL). They have reported that azi-Ru binds with the protein lysozyme through His15 and Asp87 amino acid residue. So far, numbers of experimental researches on mode of action of ruthenium-based drugs (including the hydrolysis mechanism and binding to biomolecules) have been done but to the best of our knowledge only a few computational studies have been performed at the molecular level.[19] Besker *et.al.*[20] have published a DFT study on binding nature of antitumor ruthenium(II) and ruthenium(III) complexes with DNA and protein. It is found that N7 of guanine, histidyl imidazole residue and sulfur containing methionine and cysteine residues are the preferred binding sites for ruthenium complexes. Chen *et. al.*[21] has investigated the two step hydrolysis reaction of NAMI-A by DFT method where they found that chloroaquated and *cis* diaquated species of NAMI-A is thermodynamically more stable than corresponding *trans* diaquated species. Recently, many studies have reported the stepwise mechanism of interaction of monoaquated and diaquated species of metal complexes with DNA and protein residues.[22-24]

Present work examines the stability and binding affinity of monoaqua and diaqua complexes of NAMI-A: [*trans*-$RuCl_3(H_2O)$(3H-imidazole)(DMSO-S)] (**Ia)**, [*trans*-$RuCl_2(H_2O)_2$(3H-imidazole)(DMSO-S)]$^{+1}$ (**Ib)** and its amino derivative: [*trans*-$RuCl_3(H_2O)$(4-amino-1,2,4-triazole)(DMSO-S)] (**IVa)** and [*trans*-$RuCl_2(H_2O)_2$(4-amino-1,2,4-triazole)(DMSO-S)]$^{+1}$ (**IVb)** with human serum albumin (**HSA**). Currently, it is not clear whether monoaqua or diaqua complexes or both of them are active species before reaction with protein receptor. Therefore we have considered both monoaqua and diaqua form of ruthenium(III) complexes for protein interaction. In order to find out the stability and binding affinity of anticancer drugs with protein receptor, many researchers have utilized two powerful computational strategies: docking and ONIOM (Our own N-layered Integrated molecular Orbital and Molecular Mechanics).[25-27] In the current study, to find out the appropriate orientation of the metal complex into the binding site of protein receptor, molecular docking simulations are taken up in an initial step and then quantum chemical calculations are performed using two layer ONIOM method.

5A.2.1 Computational Detail

DFT optimized geometry of **Ia**, **Ib**, **IVa** and **IVb** complexes in gas phase are obtained using unrestricted Becke's[28] three parameter hybrid exchange functional (B3) and the Lee-Yang-Parr correlation functional (LYP) (B3LYP)[29] functional with LANL2DZ + 6-31G(d,p) basis sets. LANL2DZ basis set[30] which describe effective core potential of Wadt and Hay (Los Alamos ECP) on ruthenium atom and 6-31G(d,p) basis set[31] for all other non metal atoms are used for ground state geometry optimization. LANL2DZ basis set is used as it reduces the calculation time containing larger nuclei. Vibrational analysis has been performed at the same level of theory for achieving energy minimum. GAUSSIAN 09 program package[32] is employed to carry out all the DFT calculations.

5A.2.2 Molecular docking simulation

DFT optimized structure of ruthenium complexes such as **Ia**, **Ib**, **IVa** and **IVb** and crystal structure of human serum albumin (**HSA**) entitled 1H9Z, obtained from research collaboratory for structural bioinformatics (RCSB) protein data bank are taken for molecular docking simulation. Three homologous domains of **HSA** are 1, 2, 3 each of which is composed of A and B subdomains.[33] Site 1 and site 2, located in hydrophobic cavities in subdomains 2A and 3A are the two major drug binding site of **HSA**.[33,34] Some recent investigations have demonstrated that anthanthracycline drugs bind to a non classical binding site on subdomain 1B of **HSA**.[35,36] Therefore in this study, subdomain 1B has been chosen as ligand binding site during docking simulation. Autodock 4.2 program[37], an interactive molecular graphics program is used to perform molecular docking simulation. For docking, the protein structure in pdb format is prepared by structure preparation tool available in Auto Dock Tools package version 1.5.4. All the water molecules and the residues (warfarin moieties namely Coumarin, Benzyl and Acetonyl which are found to be complexed with **HSA** receptor) have been removed from the crystal structure of **HSA** and then polar hydrogen atoms are added for saturation, Gasteiger charges are computed and non-polar hydrogen atoms are merged. A grid box with grid spacing of 0.375 Å and dimension of 60×60×60 grid points along x, y and z axes are built around the ligand binding site. The grid box carries the complete binding site of the protein receptor and gives sufficient space for the ligand translational and rotational walk. Finally, ten possible docking runs are performed with step sizes of 2 Å for translation and 50^0 for

rotation. A maximum number of energy evaluations are set to 25000 and a maximum number of 27000 GA operations are generated with an initial population of 150 individuals. The rate of gene mutation and crossover are set to 0.02 and 0.80, respectively.

5A.2.3 QM/MM calculation

The lowest energy structure, obtained from preceding docking simulation is chosen as the starting geometry for the two layer ONIOM study. The residues located outside the active site region of protein receptor are removed in order to reduce the system size. Investigation of the whole protein-ligand adduct by quantum mechanics (QM) is very computationally demanding. Hence, we have applied QM on the interacting residues with the ruthenium complex and molecular mechanics (MM) for the remaining part of the system (Fig.5A.1).

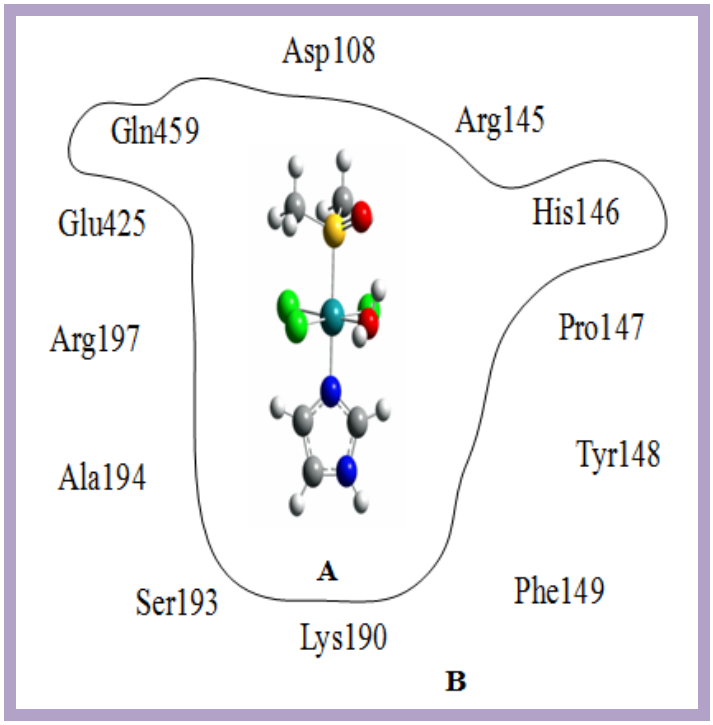

Fig. 5A.1 Schematic 2D diagram of the model system for ruthenium complex bound to **HSA** binding site. Layers that are partitioned are shown for ONIOM2 calculations. **A** is the inner layer (QM calculations) and **B** is the outer layer (MM calculations). The arrangement of the residues shown in 2D diagram is not their actual position in 3D.

For monoaquated adduct, the QM region is composed of ruthenium complex, His146 and Gln459 residue while MM region is composed of Ala194, Arg145, Arg197, Asp108, Glu425, Leu463, Phe149, Pro147, Ser193 and Tyr148 residue respectively. Here charge of both the layer is set to be 0. On the other hand, for diaquated adducts, QM part includes ruthenium complex, His146 and Ser193. Along with these two residues Lys190 (for **Ib-HSA**), Pro147 and Glu425 (for **IVb-HSA**) are included in the QM layer. The charge of QM set for diaquated adduct is set to be +1. Finally, the whole structure is optimized using two layer ONIOM method by treating QM region at UB3LYP/ (LANL2DZ+6-31G(d,p)) level. MM region is described using universal force field, implemented in GAUSSIAN 09 program.

In the two layers ONIOM method, the total energy (E_{ONIOM}) of the entire system is obtained from three independent energy calculations:

$$E^{ONIOM2} = E^{\text{high}}_{\text{model system}} + E^{\text{low}}_{\text{real system}} - E^{\text{low}}_{\text{model system}}$$

Real system contains full geometry of the molecule and is considered as MM layer while the model system contains the chemically most important (core) part of the system that is considered as QM layer.

To find the relative stability of respective adducts, we have evaluated the interaction energy, ΔE, which is given by the expression:

$$\Delta E = E_{HSA/\,Ru-complex} - E_{HSA} - E_{Ru-complex}$$

$E_{HSA/\,Ru-complex}$ is the energy of the optimized adduct of complex-**HSA**, E_{HSA} is the energy of the optimized **HSA** receptor and the $E_{Ru-complex}$ is the energy of the optimized ruthenium complexes.

To observe effect of solvation in the ruthenium complex**—HSA** interaction, single-point calculations have been performed on the interacting part of the protein by the UB3LYP functional, using LANL2DZ and 6-31G(d,p) basis sets and conductor-like polarized continuum model.[38,39] In order to reduce the calculation time, we have taken only the high level (QM) part for single point calculation.

5A. 3 Results and Discussion

5A.3.1 Structural analysis of monoaqua and diaqua complexes

Important geometrical parameters of the ruthenium complexes evaluated in gas phase are presented in Table 5A.1 and their optimized geometries evaluated by DFT at

B3LYP level are shown in Fig.5A.2. In complex **Ia**, the Ru—Cl1, Ru—Cl2, Ru—Cl3, Ru—O, Ru—N and Ru—S bond lengths are calculated to be 2.43, 2.38, 2.34, 2.21, 2.10 and 2.36 Å respectively. Ru—O bond length is found to be shorter than that of Ru—Cl bond lengths, indicating the stronger coordination ability of water ligands than that of chloride ligands. The coordinated water molecule of complex **Ia** form a hydrogen bond with DMSO oxygen atom (1.85 Å). The bond angles Cl1—Ru—O(wat1), O(wat1)—Ru—Cl2 , Cl2—Ru—Cl3 and Cl3—Ru—Cl1 of the complex **Ia** are found to be as: 80.6^0, 86.3^0,97.2^0 and 95.7^0, respectively. As a consequence of this deviation of bond angles from 90^0, the geometry about the ruthenium atom is distorted from regular octahedral structure.

Table 5A.1. Selected bond lengths (Å) and bond angles (^{0}) calculated for ruthenium(III) complexes at B3LYP level in the gas phase

Parameters	**Ia**	**Ib**	**IVa**	**IVb**
Ru—Cl1	2.43	2.34	2.41	2.32
Ru—Cl2	2.38		2.41	
Ru—Cl3	2.34	2.31	2.33	2.30
Ru—O(wat1)	2.21	2.23	2.24	2.24
Ru—O(wat2)		2.16		2.18
Ru—N1	2.10	2.10	2.10	2.09
Ru—S1	2.36	2.41	2.36	2.41
N1—Ru—S1	176.3		176.1	175.5
Cl1—Ru—Cl2	167.1		165.5	
Cl1—Ru—O(wat1)	80.6	83.9	85.1	85.6
O(wat1)—Ru—Cl2	86.3		80.5	
O(wat1)—Ru—O(wat2)		85.5		82.5
O(wat2)—Ru—Cl3		91.2		90.1
Cl2—Ru—Cl3	97.2		97.6	
Cl3—Ru—Cl1	95.7	99.8	96.9	99.9

For complex **Ib**, ruthenium atom is coordinated with two water molecules and one of the two water molecules have formed hydrogen bonding interaction with DMSO oxygen atom within a distance of 1.70 Å. Ru—O(wat1) and Ru—O(wat2) bond lengths are found to be 2.23 Å and 2.16 Å, respectively. Complex **Ib** also exhibits

pseudooctahedral configuration having Cl1—Ru—O(wat1), O(wat1)—Ru—O(wat2), (wat2)O—Ru—Cl_3 and Cl3—Ru—Cl1 bond angles are in the range of 83.9^0—99.8^0. These geometrical parameters are comparable with available experimental data. Similar geometrical parameters are also reported by Chen *et. al.* on studying the aquation of NAMI-A.[21] However, slightly higher values of bond lengths of all complexes are thought to be due to systematic errors caused by computation method, basis set and environment factors.[21] Electronic structures of complex **IVa** and complex **IVb** are found to be similar to that of complex **Ia** and complex **Ib.**

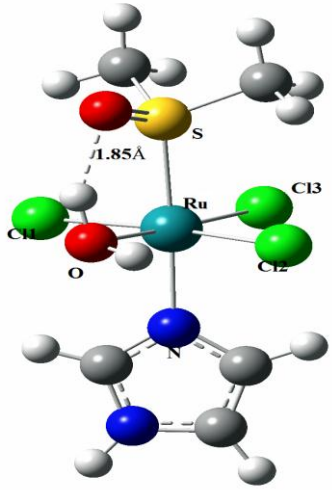

Ia

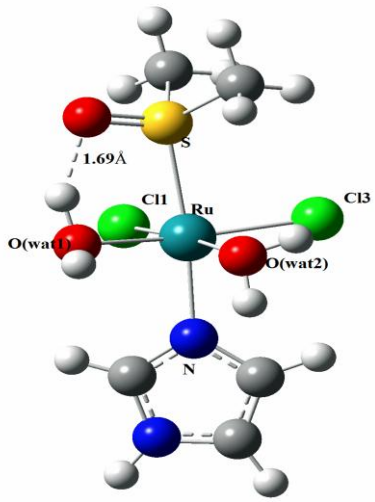

Ib

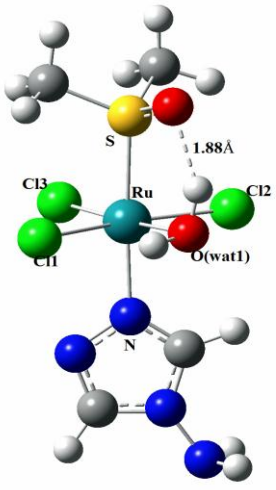

IVa

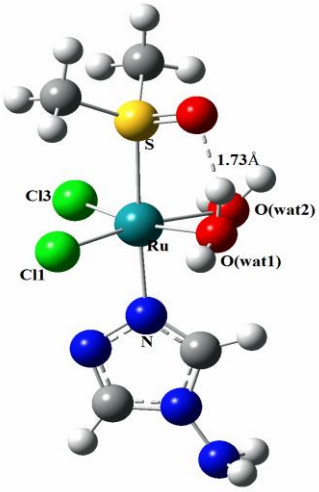

IVb

Fig.5A.2 Optimized geometries of ruthenium(III) complexes with appropriate numbering obtained from B3LYP/ (LanL2DZ+6-31G(d,p)) calculation.

5A.3.2 Stability of the ruthenium complexes

Chemical properties of ruthenium complexes are determined by analyzing the nature of highest occupied molecular orbital (HOMO) and the lowest unoccupied molecular orbital (LUMO). Calculated LUMO and HOMO energies of the ruthenium complexes are listed in Table 5A.2. With the help of LUMO—HOMO energy separation, the kinetic stability and relative reactivity pattern of a chemical system can be predicted. The lower value of energy separation indicates higher reactivity and lower kinetic stability of a molecule.[40] Pearson pointed out that the LUMO—HOMO energy separation represents the chemical hardness which is a reliable reactivity parameter to predict the stability of a molecule.[41] Greater stability of molecules is due to their higher hardness value as stated by maximum hardness principle.[42] It is observed from computational investigation that complex **Ib** (Table 5A.2) having higher value of LUMO—HOMO energy gap as well as higher chemical hardness value, exhibits higher stability than that of complex **Ia**, **IVa** and **IVb**.

Table 5A.2. Energies of HOMO (E_H in eV) and LUMO (E_L in eV) and chemical hardness (η in eV) of ruthenium(III) complexes

Complex	E_H	E_L	ΔE	η
Ia	-6.204	-3.646	2.558	1.279
Ib	-10.095	-7.335	2.758	1.379
IVa	-6.177	-3.646	2.531	1.266
IVb	-9.905	-7.510	2.395	1.198

5A.3.3…Docking study

The analysis of molecular docking calculations between ruthenium complexes with **HSA** shows that all the complexes exhibit almost similar binding orientation. The interaction energy of all the protein adducts along with their experimental binding constant (metal complexes binding to albumin) [41] are reported in Table 5A.3. The binding energy for **Ia-HSA**, **Ib-HSA**, **IVa-HSA** and **IVb-HSA** adducts are evaluated to be -4.52, -4.74, -4.58 and -4.91 kcal mol^{-1}. The larger negative value of binding energy reflects greater binding affinity of ruthenium complexes with the protein receptor. The most important amino acid components involved in binding interaction

with protein receptor are Ala194, Arg145, Arg197, Asp108, Gln459, Glu425, His146, Lys190,

Table 5A.3. Binding energy (ΔE in kcal mol^{-1}) and binding constant (k_b in min^{-1}) of all the complexes with **HSA**, evaluated by molecular docking.

Adducts	ΔE	K_b (experimental data)
Ia-HSA	-4.52	0.210
Ib-HSA	-4.74	
IVa-HSA	-4.58	0.436
IVb-HSA	-4.91	

Phe149, Pro147 and Tyr148. Docking results of ruthenium complexes are shown in Fig. 5A.3-4 and possible binding interaction of ruthenium complexes with the receptor in terms of hydrogen bond and metal-receptor interaction are presented in Table 5A.4. Fig. 5A.3 shows the binding interaction of **Ia** and **IVa** at the surface binding site of subdomain 1B. Complex **Ia** form a hydrogen bonding interaction with the amino acid residue Gln459 at a distance of about 1.90 Å through its DMSO oxygen atom and a metal receptor interaction is observed with the His146

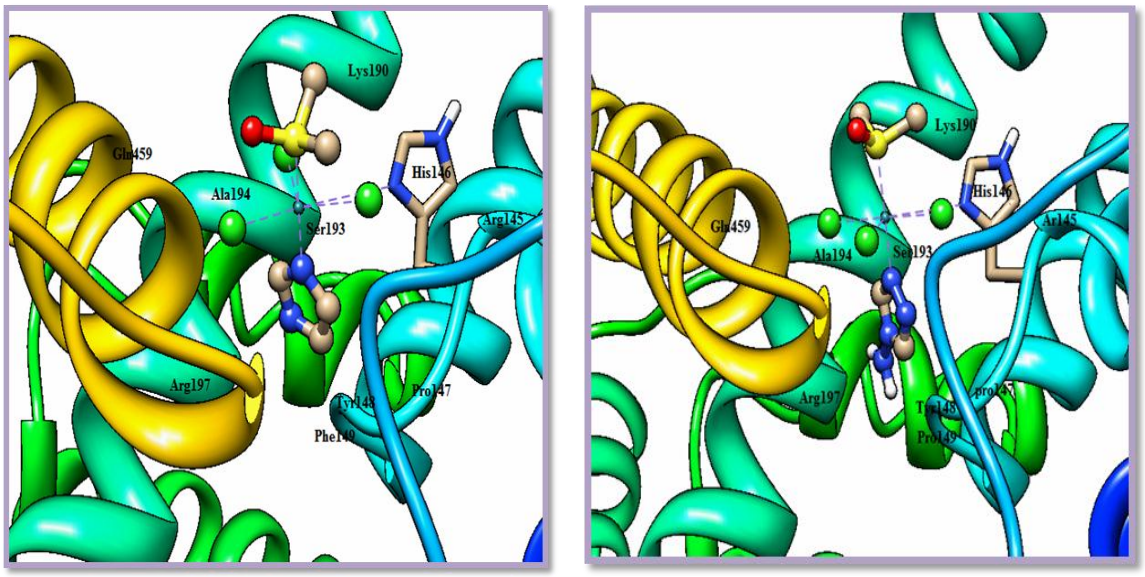

Ia–HSA **IVa–HSA**

Fig. 5A.3 Docked structures of monoaquated adducts at the active site of protein receptor. The rest part of protein structure is not shown for clarity.

residue at a distance of about 3.00 Å. A similar orientation is observed for docked structure of complex **IVa** as it shows a hydrogen bonding interaction with the amino acid residue Gln459 (1.93 Å) and a metal receptor interaction with the residue His146 (4.05 Å). Fig. 5A. 4 presents the docked structure of complex **Ib** and complex **IVb** at the active site of the protein receptor.

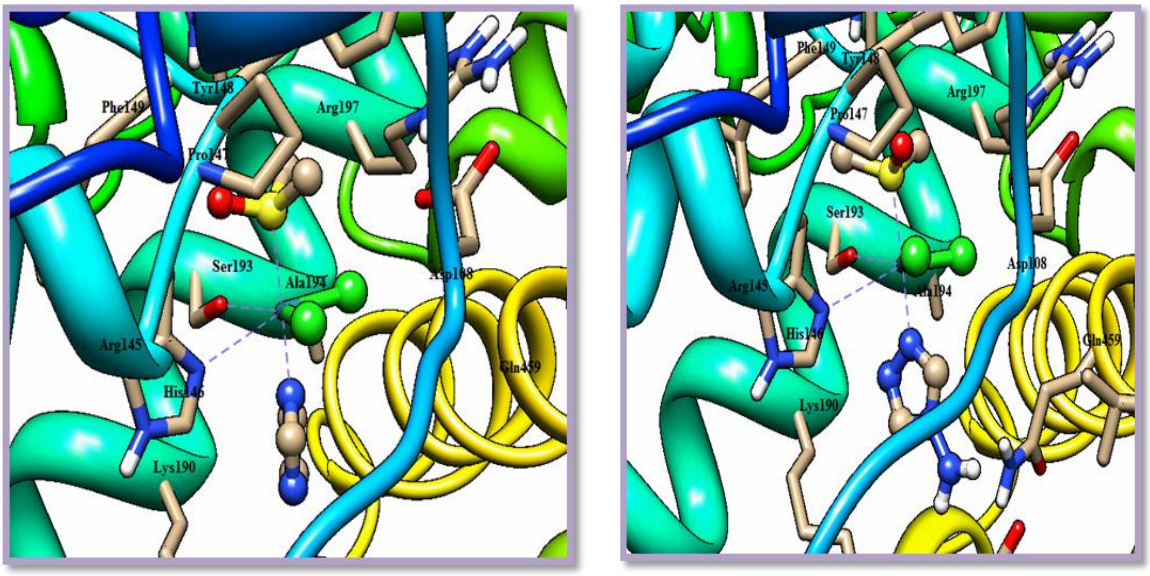

Ib–HSA **IVb–HSA**

Fig. 5A. 4 Docked structures of diaquated adducts at the active site of protein receptor. The rest part of protein structure is not shown for clarity.

Two hydrogen bonding interaction of the complex **Ib** with amino acid residue His146 (1.69 Å) and Lys190 (2.79 Å) have been observed through its DMSO oxygen atom and imidazolium hydrogen atom while only a single hydrogen bonding interaction is observed for complex **IVb** with Glu425 residue at a distance of 2.32 Å. Both the complexes form metal receptor interaction with His146 and Ser193 within a distance of 3.05 Å. As it is observed, the interaction between ruthenium complexes and **HSA** is not completely hydrophobic in nature since there are several ionic (Asp108, Glu425, Arg145, Arg197 and Lys190) and polar residues (His146, Ser193, Tyr148 and Gln459) in the proximity of the bound ligand (within 4 Å) playing crucial role in stabilizing ruthenium complexes via hydrogen bonding and electrostatic interactions.

5A.3.4 ONIOM study

5A.3.4.1 Structural Characteristics

The fully optimized structures of all the adducts of ruthenium complexes with **HSA** calculated at UB3LYP/ 6-31G (d,p): UFF level are shown in Fig. 5A.5 and significant geometrical parameters are listed in Table 5A.5.

Table 5A. 4. Hydrogen bond and metal-receptor interaction of ruthenium(III) complexes with **HSA** evaluated by docking analysis

		Amino acid residue involved in hydrogen bonding
Adducts	Groups	**HSA**
		amino acid residue
Ia–HSA	DMSO O atom	*H*NGln459(1.90Å)
	Metal-receptor	*N*-imidazole His146(3.00Å)
Ib–HSA	DMSO O atom	*H*CH_2His146(1.69Å)
	Imidazolium H atom	*O* Lys190(2.79 Å)
	Metal-receptor	*N*-imidazole His146(3.05Å)
	Metal-receptor	*O*Ser193(2.15Å)
IVa–HSA	DMSO O atom	*H*NGln459(1.93Å)
	Metal-receptor	*N*-imidazole His146(4.05Å)
IVb–HSA	Metal-receptor	*N*-imidazole His146(3.03Å)
	Metal-receptor	*O*Ser193(2.57Å)
	Imidazole H atom	*O* Glu425(2.32 Å)

Monoaqua interaction

From Fig. 5A.5 and Table 5A.5, it is seen that inside the binding site of **HSA**, complex **Ia** has retained its pseudooctahedral configuration, in which water ligand has been replaced from the system by histidyl residue and coordinated with the ruthenium atom at a distance (Ru—N_{His}) of 2.18Å. The Ru—Cl bond lengths are in the range of 2.38-2.42 Å whereas Ru—N and Ru—S bond lengths are 2.11 and 2.43 Å, respectively. It is also observed that complex **Ia** forms a hydrogen bond between DMSO oxygen atom and one of the hydrogen atoms of glutamine side chain. The existence of the hydrogen bonding in this adduct is indicated by the two important aspects: (i) short DMS<u>O</u>—H_{Gln}, contact distance of 2.03 Å (ii) deviations of

Cl1—Ru— N_{His} (85.7°) and Cl2—Ru— N_{His} **(**88.1°) bond angle from the octahedral 90° value. Presences of hydrogen bonding gives additional stability to this adduct. The calculation shows that the dihedral angle Cl3—Cl2—N_{His}—C of **Ia–HSA** is 91.5^0 which indicate that histidyl ring is found to be perpendicular to the molecular plane about its central axis. Electronic structures of **Ia–HSA** and **IVa–HSA** are found to be similar but Ru—N_{His} bond is slightly longer in **IVa–HSA**, indicating a weaker coordination ability of complex **IVa** as compared to complex **Ia**. The dihedral angle Cl3—Cl2—N_{His}—C of **IVa–HSA** is found to be 47.6^0 reflecting a deviation of histidyl ring from molecular plane.

Diaqua interaction

In **Ib–HSA,** the ruthenium atom is coordinated with histidyl nitrogen atom and oxygen atom of serine residue of protein receptor at a distance of 2.18 and 1.89 Å. The angle Cl1—Ru—N_{His} is 84.1^0 whereas the angle O_{Ser}—Ru— N_{His} is 88.8^0. This observed deviation of bond angles from 90^0 clearly indicates a distortion of geometry from regular octahedral structure. Complex **Ib** form two intermolecular hydrogen bonding with the protein receptor: DMSO—H_{His} at 2.06 Å and Imidazolium CH—O_{Lys} at 2.28 Å. The geometrical parameters of **Ib–HSA** and **IVb–HSA** are almost similar but the latter one is stabilized by presence of two additional hydrogen bonding with glutamic acid residue via imidazolium hydrogen atom. The dihedral angle (Cl3—O—N_{His}—C) of **Ib–HSA** is found to be 116.7^0 and for **IVb-HSA** is 94.7^0.

Table 5A.5. Calculated bond length (Å) and bond angles (^{0}) of monoaquated and diaquated adduct

	Ia-HSA		**IVa-HSA**		**Ib-HSA**		**IVb-HSA**	
	Ru-coordination	Hydrogen bonding	Ru-coordination	Hydrogen Bonding	Ru-coordination	Hydrogen bonding	Ru-coordination	Hydrogen bonding
Ru—N_{His}	2.18		2.25		2.18		2.16	
Ru—O_{Ser}					1.89		1.99	
Ru—Cl1	2.42		2.45		2.38		2.38	
Ru—Cl2	2.40		2.38					
Ru—Cl3	2.38		2.36		2.34		2.47	
Ru—S	2.43		2.42		2.48		2.37	
Ru—N	2.11		2.10		2.14		2.16	
DMS<u>O</u>—H_{Gln}		2.03		1.98				
DMS<u>O</u>—H_{His}						2.06		2.43
Imidazolium<u>C</u>H—O_{Lys}						2.28		
DMSOCH_2<u>H</u>—O_{Ser}						2.50		2.28
Imidazolium<u>N</u>H—O_{Glu}								1.88
Imidazolium<u>C</u>H—O_{Glu}								2.04
Cl1—Ru— N_{His}	85.7		87.2		84.1		94.9	
Cl2—Ru— N_{His}	88.1		93.5					
Cl2—Ru— Cl3	92.8		91.5					
Cl3—Ru— Cl1	93.4		87.8		92.6		85.2	
O_{Ser}—Ru— N_{His}					88.8		87.8	
O_{Ser} —Ru— Cl3					95.5		92.1	
Cl3—Cl2—N_{His}—C	91.5		47.6					
Cl3—O—N_{His}—C					116.7		94.7	

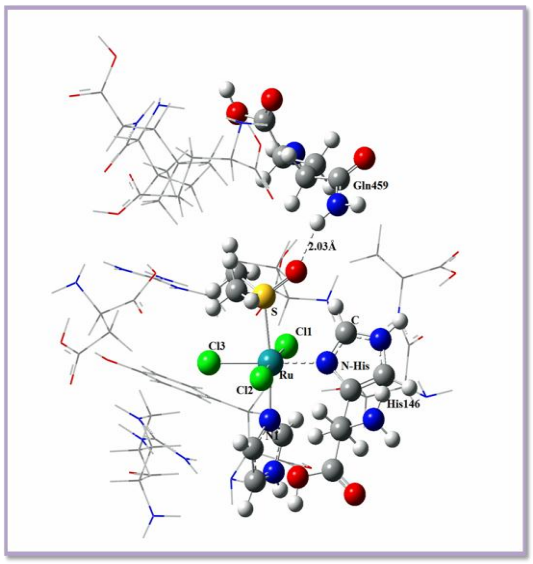

Ia–HSA

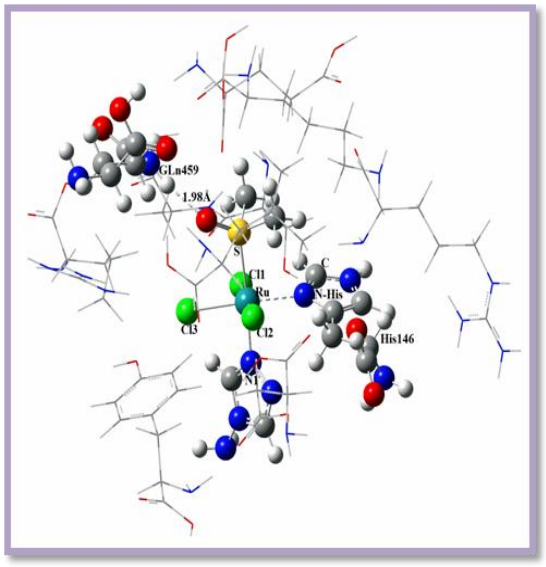

IVa–HSA

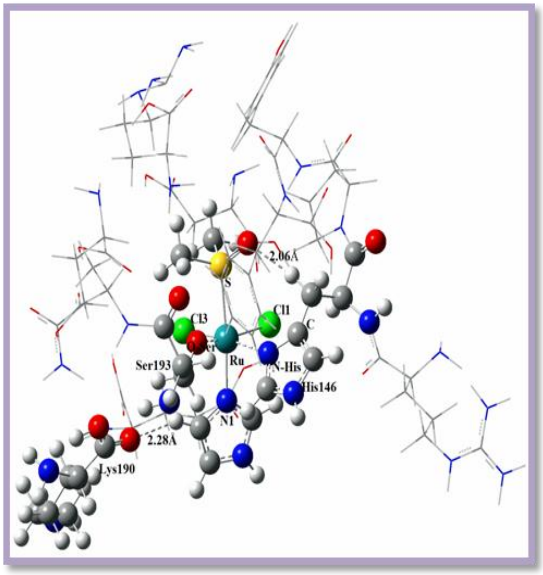

Ib–HSA

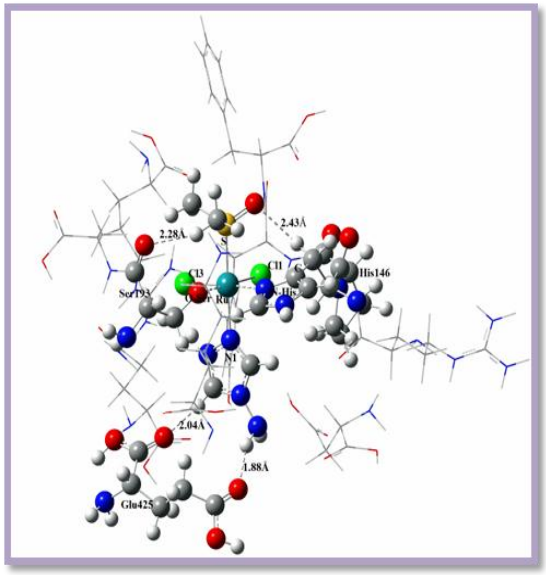

IVb-HSA

Fig.5A.5. Optimized geometries of monoaquated and diaquated adducts with appropriate numbering obtained from two layer QM/MM method.

5A.3.4.2 Stability

In order to find out the stability of the four adducts we have evaluated the binding energy which are presented in Table 5A.6 along with the absolute energy values of the interacting moieties. The results shown in Table 5A.6 allow us to conclude that the binding energies of diaqua adducts are higher than that of monoaqua adducts. That is diaqua adducts are more stable than the corresponding monoaqua adducts.

Table 5A.6. Absolute energy values (in a.u.) of interacting adducts and calculated binding energy ($\Delta E \times 10^2$ in kcal mol^{-1}) of ruthenium complexes with **HSA** calculated by two layer ONIOM method in gas phase. Interacting part of **HSA** in aqueous phase is calculated by high level UB3LYP/(LANL2DZ+6-31G(d,p)) method.

Adduct	Gas phase				Solvent phase			
	$E_{HSA/Ru-complex}$	E_{HSA}	$E_{Ru-complex}$	ΔE	$E_{HSA/Ru-complex}$	E_{HSA}	$E_{Ru-complex}$	ΔE
Ia–HSA	-3333.57	-1080.52	-2330.49	479.67	-3334.66	-1080.58	-2330.52	479.70
Ib–HSA	-3087.34	-1293.53	-1946.47	958.50	-3087.34	-1293.65	-1946.56	959.23
IVa–HSA	-3405.91	-1080.52	-2401.83	479.62	-3405.99	-1080.58	-2401.86	479.69
IVb–HSA	-3538.64	-1672.88	-2017.81	954.12	-3538.68	-1672.92	-2017.98	954.68

Again, **IVb–HSA** have lowest absolute energy value ($\Delta E_{HSA/\,Ru-complex}$), suggesting that this diaqua form of amino derivative of NAMI-A has higher reactivity towards protein receptor, in agreement with the experimental studies reported by Grossl *et al*.[43] This is mainly due to the presence of primary amine group in this derivative which favors formation of hydrogen bonding interaction towards protein residues, making protein—complex conjugation. In spite of its higher reactivity towards protein receptor, the evaluated binding energy of **IVb–HSA** adduct is lower as compared to **Ib**–**HSA** and hence exhibited less stability than that of **Ib**–**HSA**. **Ib–HSA** having energy 958.50×10^{2} kcal mol^{-1} being the most stable adduct followed by **IVb–HSA**, **Ia–HSA** and **IVa–HSA**.

Since all biological interactions are occur in aqueous environments, we have carried out single point calculations on interacting part of all the four adducts to get an estimate of the solvent effect. Inclusion of solvent effect in energy calculations lead to changes in energy and stability of the corresponding adducts. The order of binding energy in aquous solution is found to be in the order: **Ib–HSA> IVb–HSA**> **Ia–HSA**> **IVa–HSA**. The binding energies of all adducts are evaluated to be higher compared to their respective counterpart in gas phase, indicating the increased stability of all the adducts with the inclusion of solvent medium.

5A.4 Conclusion

Molecular docking and QM/MM calculation has been carried out for monoaqua and diaqua ruthenium(III) complexes in order to evaluate the binding affinity and stability of the complexes in protein environment. Molecular docking simulation shows that diaqua adduct i.e., **Ib–HSA** and **IVb–HSA** has exhibited higher binding affinity than the corresponding monoaqua adducts (**Ia–HSA** and **IVa–HSA**). These studies reveal that in the active site of protein, residues Ala194, Arg145, Arg197, Asp108, Gln459, Glu425, His146, Lys190, Phe149, Pro147 and Tyr148 play a key role in binding with the complexes. In monoaqua adducts, ruthenium complex are found to interact with His146 and Gln459 while ruthenium complexes in diaqua adducts interact with Ser193, Lys190 and Glu425 in addition to His146. Again, two layer ONIOM calculations analyze the stability and energetic details of the interacting ruthenium complexes with protein. The binding energy evaluated by ONIOM calculation suggests the highest stability of **Ib–HSA** adduct. However, interaction energy of

IVb–HSA adduct is higher than other adduct indicating higher reactivity of complex **IV** towards protein, in agreement with experimental data. Binding energy values suggest that diaqua adducts is more stable than monoaqua adducts. Presence of more hydrogen bonding in diaqua adducts gives extra stability as compared to monoaqua adducts. In addition, the interaction energies of all the four adduct increases in water solvent.

References

1. V. Brabec, O. Novakova, *Drug Resistance Update*, 2006, **9**, 111-122.
2. O. Novakova, J. Kasparkova, O. Vrana, P. M. Van Vliet, J. Reedijk, V. Brabec, *Biochemistry*, 1995, **34**, 12369-12378.
3. C. G. Kuehn, H. Taube, *J. Am. Chem. Soc.*, 1976, **98**, 689. S .Fruhauf, W. Zeller, *Cancer Res.*, 1991, **51**, 2943-2948.
4. K. Hindmarsh, D. A. House, M. M. Turnbull, *Inorg. Chim. Acta*., 1997, **257**, 11–18.
5. L. G. Marzilli, S .O. Ano, F. P. Intini, G. Natile, *J. Am. Chem. Soc.*, 1999, **121**, 9133–9142.
6. J. Arpalahti, M. Mikola, S. Mauristo, *Inorg. Chem.*, 1993, **32**, 3327–3332.
7. L. Messori, F. Gonzales Vilchez, R. Vilaplana, F. Piccioli, E. Alessio, B. K. Keppler, *Met.-Based Drugs*., 2000, **7**, 335-342.
8. F. Piccioli, S. Sabatini, L. Messori, P. Orioli, C. G. Hartinger, B. K. Keppler, *J. Inorg. Biochem.*, 2004, **98**, 1135-1142.
9. P. T. Gomme, K. B McCann, K. B Bertolini, J. *Drug Discovery Today,* 2005, **10**, 267-273.
10. E. Reisner, V. B. Arion, C. G. Hartinger, M. A. Jakupec, A. J. L. Pombeiro, B. K. Keppler, *in: A.M. Trzeciak (Ed.), Education inAdvanced Chemistry, Wydawnictwo Uniwersytetu Wroctawskiego,* n-Wrocław, 2005, Vol. 9, pp 215-229.
11. K. Polec-Pawlak, J. K. Abramski, O. Semenova, C. G. Hartinger, A. R. Timerbaev, B. K Keppler, M Jarosz, *Electrophoresis*, 2006, **27**, 1128-1135.
12. M. J. Clarke, F. Zu, D. R. Frasca, *Chem. Re*v., 1999, **99**, 2511-2533.
13. M. J. Clarke, *Coord. Chem. Rev*., 2002, **232**, 69-93.
14. D. Frasca, M. J. Clarke, *J. Am. Chem. Soc.*, 1999, **121**, 8523-8532.
15. M. Zhao, M. J. Clarke, *J. Biol. Inorg. Chem.*, 1999, **4**, 318-340.
16. C. A. Smith, A. J. Sutherland-Smith, B. K. Keppler, F. Kratz, E. N. Baker, *J. Biol. Inorg. Chem.*, 1996, **1**, 424-431.
17. A. Casini, C. Temperini, C. Gabbiani, C. T. Supuran, L. Messori, *ChemMedChem.*, 2010, **3**, 1989-1994.
18. A. Vergara, G. D'Errico, D. Montesarchio, G. Mangiapia, L. Paduan, A. Merlino, *Inorg. Chem.*, 2013, **52**, 4157-4159.

19. J-C. Chen, L-M. Chen, L-C. Xu, K-C. Zheng, L-N. Ji, *J. Phys. Chem. B*, 2008, **112**, 9966–9974.

20. N. Besker, C. Coletti, A. Marrone, N. Re, *J. Phys. Chem. B*, 2007, **111**, 9955-9964.

21. J. Chen, L. Chen, S. Liao, K. Zheng, L. Ji, *J. Phys. Chem. B*, 2007, **111**, 7862-7869.

22. S. Banerjee, A. K. Mukherjee, *Inorg. Chim. Acta.*, 2013, **400**, 130–141.

23. Q. Fu, L. Zhou, J. Li, *Struct Chem*, 2012, **23**, 1931–1940.

24. P. Sarmah, R. C. Deka, *J Mol Struct: Theochem*, 2010, **955**, 53-60.

25. T. Yoshida, Y. Munei, S. Hitaoka, H. Chuman, *J. Chem. Inf. Model.*, 2010, **50**, 850–860.

26. J. H. Alzate-Morales , J. Caballero , F. D. Gonzalez-Nilo, R. Contreras, *Chem. Phys. Lett.*,2009, **479**, 149-155.

27. J. H. Alzate -Morales, J. Caballero, A. V. Jague, F. D. Gonzalez -Nilo, *J. Chem. Inf. Model.*, 2009, **49**, 886–899.

28. A. D. Becke, *Phys. Rev. A*, 1988, **38**, 3098-3100.

29. C. Lee, W. Yang, R. G. Parr, *Phys. Rev.*, 1988, **37**,785-789.

30. P. J. Hay, W. R. Wadt, *J. Chem. Phys.*, 1985, **82**, 270-284.

31. P. C. Hariharan, J. A. Pople, *Chem. Phys. Lett.*, 1972, **16**, 217-219.

32. M. J. Frisch, G. W. Trucks, H. B. Schlegel, G. E. Scuseria, M. A. Robb, J. R. Cheeseman, G. Scalmani, V. Barone, B. Mennucci, G. A. Petersson, H. Nakatsuji, M. Caricato, X. Li, H. P. Hratchian, A. F. Izmaylov, J. Bloino, G. Zheng, J. L. Sonnenberg, M. Hada, M. Ehara, K. Toyota, R. Fukuda, J. Hasegawa, M. Ishida, T. Nakajima, Y. Honda, O. Kitao, H. Nakai, T. Vreven, J .A. Montgomery, J. E. Peralta, F .Ogliaro, M. Bearpark, J. J. Heyd, E. Brothers, K. N. Kudin, V. N. Staroverov, T. Keith, R. Kobayashi, J. Normand, K. Raghavachari, A. Rendell, J. C. Burant, S. S. Iyengar, J .Tomasi, M. Cossi, N. Rega, J. M. Millam, M. Klene, J. E. Knox, J. B. Cross, V. Bakken, C. Adamo, J. Jaramillo, R. Gomperts, R. E. Stratmann, O. Yazyev, A. J. Austin, R. Cammi, C. Pomelli, J. W. Ochterski, R. L. Martin, K. Morokuma, V. G. Zakrzewski, G. A. Voth, P. Salvador, J. J. Dannenberg, S. Dapprich, A. D. Daniels, O. Farkas, J. B. Foresman, J. V. Ortiz, J. Cioslowski, D. J. Fox, Gaussian 09 (Revision B.01), Gaussian Inc., Wallingford, CT, 2010.

33. D. C. Carter, J. X. Ho, *Adv. Protein Chem.*, 1994, **45**, 153–203.

34. G. Sudlow, D. J. Birkett, D. N. Wade, *Mol. Pharmacol.*, 1976, **12**, 1052–1061.

35. K. Tang, Y-M. Qin, A-H. Lin, X. Hu, G.-Lin Zou, *J. Pharm. Biomed. Analysis*, 2005, **39**, 404–410.

36. S. N. Khana, B. Islama, R. Yennamalli, A. Sultana, N. Subbarao, A. U. Khana, *Eur. J. Pharm Sc.*, 2008, **35**, 371–382.

37. G. M. Morris, R. Huey, W. Lindstrom, M. F. Sanner, R. K. Below, D. S. Goodsell, A. J. Olson, *J. Comput. Chem.*, 2009, **30**, 2785-2791.

38. V. Barone, M. Cossi, *J. Phys. Chem. A*, 1998, **102**, 1995-2001.

39. M. Cossi, N. Rega, G. Scalmani, V. Barone, *J. Comp. Chem*., 2003, **24**, 669-681.

40. J. I. Aihara, *J. Phys. Chem. A*, 1999, **103**, 7487–7495.

41. R. G. Pearson, *Hard and soft acids and bases*, Dowden, Hutchinson, Ross, Stroudsburg, PA, 1973.

42. R. G. Pearson, *J. Chem. Educ*., 1987, **64**, 561–567.

43. M. Grossl, E. Reisner, C. G. Hartinger, R. Eichinger, O. Semenova, A. R. Timerbaev, M. A. Jakupec, V. B .Arion, B. K. Keppler, *J. Med. Chem.*, 2007, **50**, 2185-2193.

INTERACTION MECHANISM OF AQUATED FORM OF RUTHENIUM(III) ANTICANCER COMPLEXES WITH HISTIDINE AND CYSTEINE

5B.1 Introduction

Three dimensional protein structures are built up with 20 natural amino acids. Each of them has its unique structural characters and physicochemical properties. Among these amino acids, histidine (His, H) plays an important role in the protein architectures and bioactivities.[1-4] Histidine is mainly present in the active sites of several metalloenzymes[5], hence lead to numerous studies involving the binding of histidine residue to metal ions.[6] The versatility of histidine in molecular interactions arises because of its unique molecular structure.[7] It has been observed that imidazole nitrogen of histdine residues is the main center by which metal ions bound to proteins.[8] The basic nitrogen atom in the imidazole of histidine has a lone electron pair which make it coordination to metallic cations. More recently Vergara *et. al*. and Casini *et. al*. provides structural evidence for the involvement of histidine residue to bind with the ruthenium(III) complexes including NAMI-A, NAMI-A analogue called azi-Ru etc., as already mentioned in chapter 5A. We have investigated the interactions of human serum albumin with NAMI-A by molecular docking simulation and found to bind the complex with histidine residue. The investigations are discussed in detail in chapter 5A.

The three potential histidine binding sites for ruthenium on horse heart cytc are His33, His26, and His18. His33 is the surface residue of protein, His 26 is an interior residue within the protein while His18 is a residue bound to the heme iron.[9] Hydrophilic complexes like $[Ru(NH_3)_5(OH)_2]^{2+}$ and $[Ru(NH_3)_4L(OH_2)]^{2+}$ (L is a nitrogen heterocycle) is found to bind to His33[10-13] whereas hydrophobic ruthenium(II) aquobipyridine complexes like *cis*-$[Ru\text{-}(bpy)_2(H_2O)_2]^{2+}$ (bpy =2,2$^{/}$-bipyridine) covalently binds to both His33 and His26 residues of horse heart cytc.[14]

On the other hand, sulphur-containing amino acids like methionine and cysteine are also play a major role in binding with the complexes. In the cases of cysteine amino acid interaction, metal atoms such as Ru, Pt etc. forms a strong dative bonds with S atoms according to HSAB (Hard–Soft-Acid–Base) principle[15,16], as these atoms (sulphur, ruthenium or platinum atom as well as most of the transition metals) belong to the so called soft atoms with a relatively high polarizability. Interactions between

such atoms are generally considered to be strong, hence, can be expected that cysteine will play an important role in the transition metal complex metabolism. This assumption of metabolism was confirmed when the $Pt(L–Met–S,N)_2$ type of complex had been recognized in the patient's urine after cisplatin administration.[17]

Mutation of tumor suppressor gene, p53, plays major role in a wide range of biochemical processes including: cell cycle regulation, DNA repair etc.[18] But it is also a common cause of wide variety of human cancers.[19-22] Experimental reports shows that involvement of cysteine residues suppresses the transactivation and transformation functions of p53.[23] Another significant role of cysteine is activation of macrophage migration inhibitory factor, MIF, a protein which involved in cell-mediated immunity, immuno-regulation and inflammation.[24] An investigation of the reactivity of NAMI-A and NAMI-A type of complexes with cysteine is therefore of high biological relevance.

The present work focuses exclusively on substitution of aqua ligand from monoaqua and diaqua form of NAMI-A type anticancer complex with histidine and cysteine by DFT method to shed light on its binding mechanism with protein receptors (Scheme1). N3 site of histidine and S site of cysteine are considered as the potential coordination site of ruthenium complexes in this study.

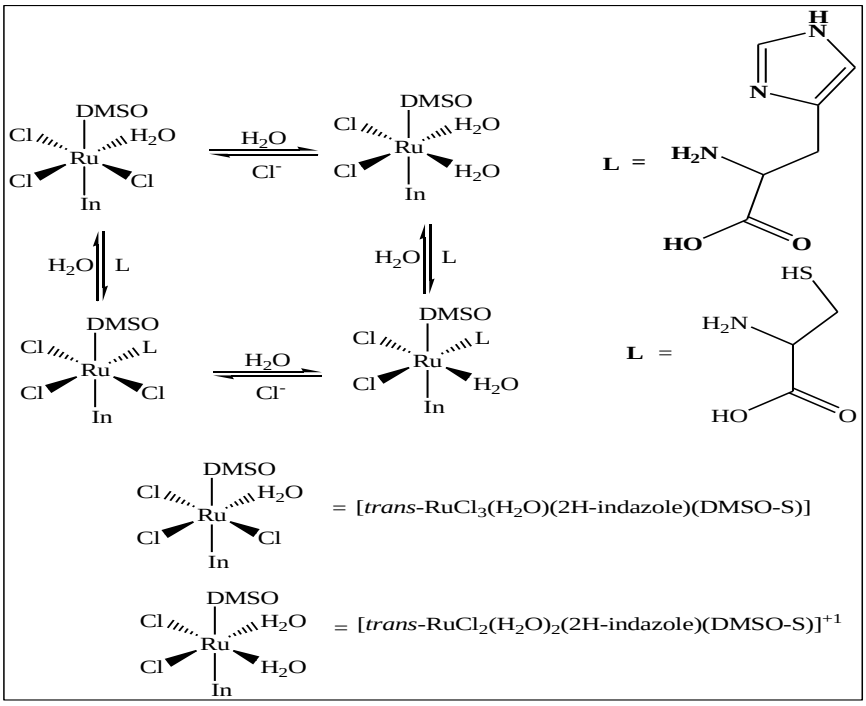

Scheme1 Proposed interaction mechanism of ruthenium(III) complex with histidine and cysteine.

5B. 2 Computational Methods

All computations reported in this discussion were carried out by using density functional theory (DFT) method as implemented in DMOL3 package.[25] Ground state geometry optimization of all the stationary points involved in interaction mechanism of ruthenium(III) complexes with histidine and cysteine were performed using Becke-Lee-Yang-Parr (BLYP)[26,27] exchange correlation functional and the double numerical with polarization (DNP)[28] basis set in combination with generalized gradient approximation (GGA). DNP basis set considers a polarization d function on heavy atoms and a polarization p function on hydrogen atoms. This basis set is comparable to the split-valence double zeta 6-31G(d,p) in size; but more accurate than the Gaussian basis sets of the same size.[29,30] A smearing of 0.005 Ha (1 Ha 5 27.21 eV) was used for the occupation of the electronic levels to achieve accurate electronic convergence. The spin-unrestricted method was used and the real-space global cutoff radius was set to be 4.70 Å for all calculations. Hessian calculations for obtaining the vibrational frequencies were performed at the same level of theory on optimized geometry to check whether the stationary points on the potential energy surface of the molecular systems are an energy minimum (with no imaginary frequency) or transition state (with only one imaginary frequency). Harmonic vibrational frequency calculations were also performed in order to obtain thermal corrections to free energies at 298.15K. The transition states for all the stationary points were obtained through the synchronous transit method[31] with conjugated gradient refinements (LST/QST tools) implemented in DMol3 code. The synchronous transit method involves linear synchronous transit (LST) maximization, followed by repeated conjugated gradient (CG) minimizations, and then quadratic synchronous transit (QST) maximizations and repeated CG minimizations until a transition state is located. The transition state that was obtained by the synchronous transit method may not be the transition state connecting the intended reactant and product for a particular reaction. Hence, to investigate the reaction path thoroughly, the intrinsic reaction coordinate (IRC) analysis was performed. The IRC calculations are incorporated in the Transition State Confirmation tool in DMOL3.[32] The Conductor-like Screening Model (COSMO) as incorporated into the DMOL3 program with a dielectric constant of 78.4 is adopted to simulate the solvent (water) environment.[33]

The rate constants for all the substitution reactions are calculated with the help of transition state theory formalism[34] proposed by Eyring as

$$k(T) = \frac{K_B T}{h} e^{-\Delta G^{\neq} / RT}$$

Where K_B is the Baltzmann constant, T is the absolute temperature and $\Delta G^{\neq}$ is the activation free energy.

Free energies and enthalpies in solvent medium are calculated with the following equations:[35]

$$G_{solv} = G_{solvent} - G_{gas}$$

$$H(aq) = H\ (g) + G_{solv}$$

$$G(aq) = G(g) + G_{solv}$$

Where G_{solv} is the solvation free energy, H is the enthalpy and G is the Gibbs free energy.

5B. 3 Results and Discussion

5B.3.1 Structural Characteristics

Fully optimized structures of all the species involved in the ligand exchange reaction of ruthenium(III) complexes; [*trans*-$RuCl_3(H_2O)$(2H-indazole)(DMSO-S)] (**IIa**) and [*trans*-$RuCl_3(H_2O)$(2H-indazole)(dmso-S)]$^{+1}$ (**IIb**) with histidine and cysteine calculated at BLYP/DNP level are presented in Fig.5B.1 and Fig.5B.2, respectively. Important geometrical parameters of all the intermediates and transition states are presented in Table 5B.1 and Table 5B.2. It has been observed that all the reactants and products acquired pseudooctahedral geometry around the ruthenium atom.

Monoaqua complex binding to histidine and cysteine

From Fig.5B.1 and Table 5B.1, it is seen that in the intermediates, **R1** and **R2**, the histidine and cysteine molecules approach the reaction center via hydrogen bonding with the adjacent H1 atom of water molecule at a distance of 1.78 Å (N3···HOH) and 2.37 Å (S···HOH), respectively. Pentagonal bipyramidal transition states (**TS1** and **TS2**) are found for the substitution of aqua ligand from monoaqua ruthenium complex with histidine and cysteine which are confirmed by the presence of one imaginary frequency each. The Ru—N3 bond distance is reduces from 4.46 Å in **R1** to 3.55 Å in

Table 5B.1 Optimized Geometric parameters (bond length in Å and bond angles in ^{0}) of all the stationary points in ligand exchange reaction of **IIa** with histidine and cysteine at the level of BLYP/DNP in gas phase.

Parameters	**First intermediate**		**Transition state**		**Second intermediate**	
	R1	**R2**	**TS1**	**TS2**	**P1**	**P2**
Ru—N3	4.43		3.55		2.22	
Ru—S		4.86		4.70		2.54
Ru—O	2.21	2.24	5.65	4.11		
N3—Ru—O			45.6			
S—Ru—O				44.7		
Cl1—Ru—O						
Cl1—Ru—N3					85.5	
Cl1—Ru—S						84.6
N3—H1(wat)	1.78					
S—H1(wat)		2.37				
O(wat)—H5					1.91	
O(wat)—H1(Cys)				2.38		2.42
O(DMSO)—H2(wat)			2.82	2.75		

TS1, while Ru—O(wat) bond distance increases from 2.21 to 5.65 Å, hence it follows a dissociative mechanism. Similar variations of bond distances are observed for **TS2**. The structures of intermediates **P1**and **P2** are observed to be pseudooctahedral, in which water ligand is completely exchanged by histidine or cysteine and forms a bond with Ru^{3+} ion at distance of 2.22 Å and 2.54 Å, respectively. The leaving water molecule makes hydrogen bonding with N5 atom of histidine at a distance of 1.91 Å and cysteine at distance of 2.42 Å.

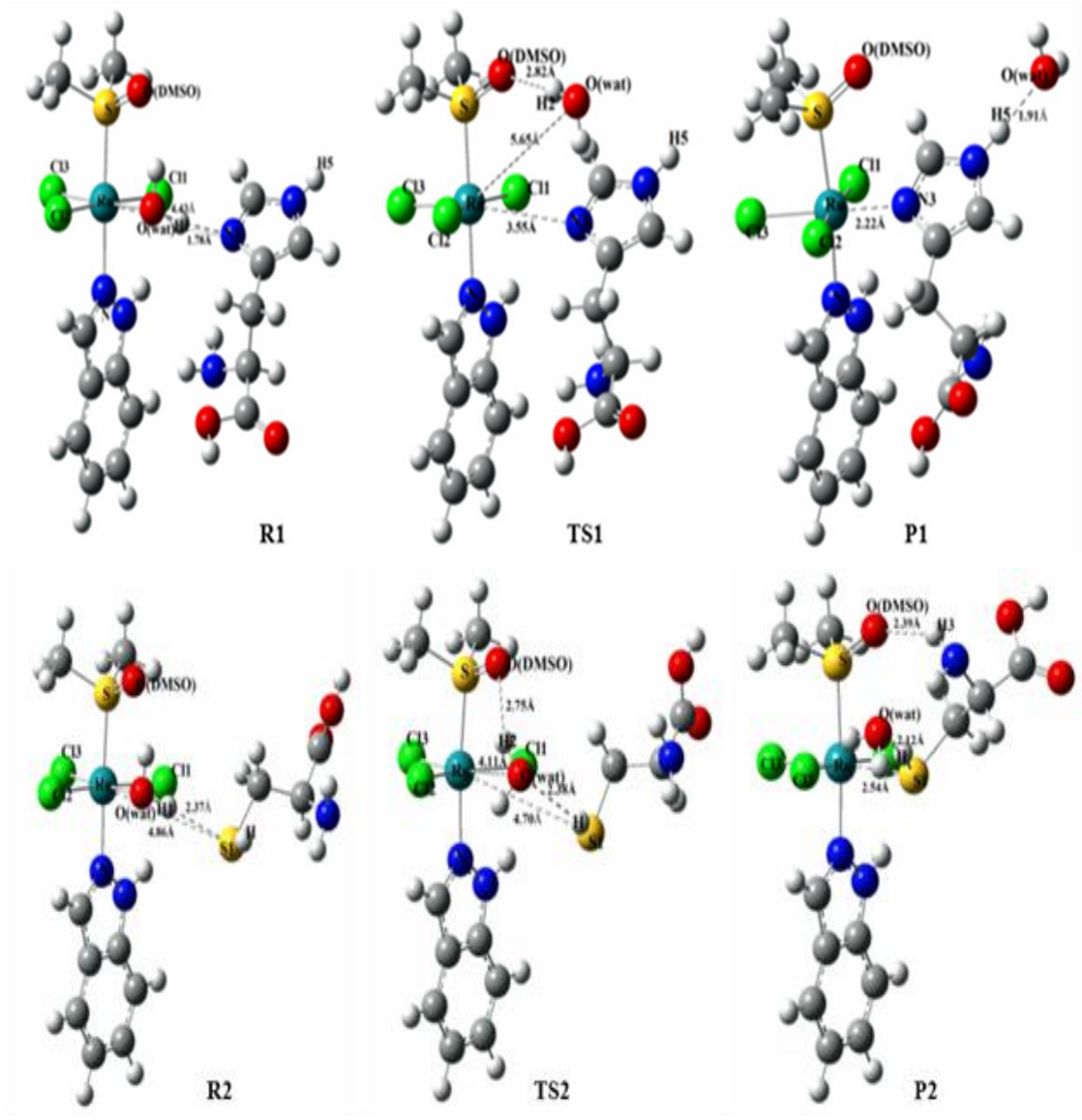

Fig.5B.1 Optimized structures of **R**, **TS**, and **P** for interactions of **IIa** with histidine and cysteine calculated at BLYP/DNP level.

Diaquated complex binding to histidine and cysteine

The optimized stationary points found for the diaqua complex [*trans*-$RuCl_2(H_2O)_2$(2H-indazole)(dmso-S)]$^{+1}$ (**IIb**) with histidine and cysteine ligands are found to be quite similar to those for monoaquated complex (shown in Fig. 5B.2.). In **R1**$^{/}$, the distance between the attacking N3 atom of histidine and Ru atom is 4.46 Å while, the Ru—S (cysteine) bond length in **R2**$^{/}$ is found to be 4.25 Å. There is an intermolecular hydrogen bonding between histidine N3 atom and H1 atom of water molecule in **R1**$^{/}$ at a distance of 1.67 Å. Presence of hydrogen bonding gives extra stability to **R1**$^{/}$ complex. In **TS1**$^{/}$, the entering histidine residue approaches the reaction center where Ru—his distance decreases from 4.46 Å to 3.97 Å, while, the leaving water ligand moves from the reaction center with Ru—O distance increases from 2.17 to 4.55 Å, indicating a. dissociative character of the transition state. In the **TS2**$^{/}$ structure also, the Ru—O(wat1) distance increases and Ru—S distance correspondingly reduced when compared with **R2**$^{/}$. Similar to the mono aqua ruthenium complexes seven coordinated unstable transition states are also obtained for diaqua ruthenium complexes. In the second intermediate **P1**$^{/}$, bond length Ru—N3(histidine) is observed to be 2.20 Å and the expelled H_2O molecule lies at a distance 6.88 Å, while, in **P2**$^{/}$, the bond distance Ru—S(cysteine) is found to be 2.82 Å and the leaving water ligand stays at distance of 5.69Å from the Ru atom. It is also observed from Table 5B.2 that H5 atom of histidine and H atom of cysteine forms hydrogen bond with the leaving water molecule at distances 1.83 Å and 1.77 Å, respectively

.

Table 5B. 2 Optimized Geometric parameters (bond length in Å and bond angles in ^{0}) of all the stationary points in ligand exchange reaction of **IIb** with histidine and cysteine at the level of BLYP/DNP in gas phase.

Parameters	**First intermediate**		**Transition state**		**Second intermediate**	
	R1$^{/}$	**R2$^{/}$**	**TS1$^{/}$**	**TS2$^{/}$**	**P1$^{/}$**	**P2$^{/}$**
Ru—N3	4.46		3.97		2.20	
Ru—S		4.25		3.45		2.82
Ru—O1	2.17	2.16	4.55	4.93	6.88	5.69
N3—Ru—O(wat2)	64.7		64.4		86.1	
S—Ru—O(wat2)		48.7		62.1		83.3
Cl1—Ru—O						
N3—H1(wat1)	1.67				85.5	
Cl1—Ru—S						84.6
N3—H1(wat)	1.78					
S—H1(wat)		2.37				
O(wat)—H5					1.83	
O(wat)—H(Cys)						1.77
O(DMSO)—H2(wat1)	1.92	2.03				

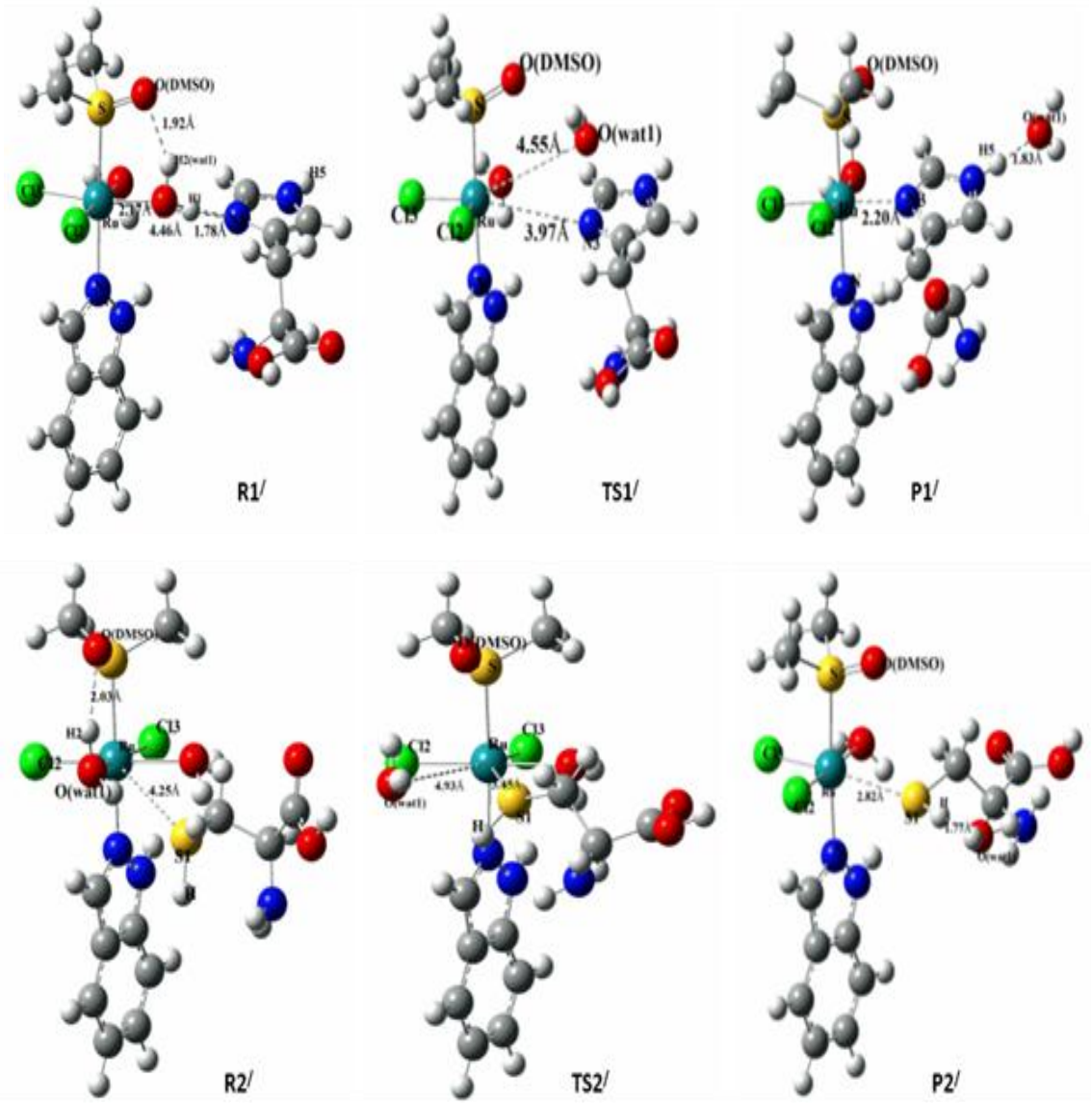

Fig.5B.2 Optimized structures of **R**, **TS**, and **P** for interactions of **IIb** complex with histidine and cysteine calculated at BLYP/DNP level.

5B.3.2 Energy Profiles of ligand exchange reaction

Monoaqua complex binding to histidine and cysteine

Change of enthalpies (ΔH), Gibbs free energies (ΔG) and solvation energies (G_{solv}) of the stationary points for the water exchange reaction of monoaqua ruthenium(III) complex **IIa**, with histidine and cysteine at 298.15K in the gas and solvent phases calculated at BLYP-DNP level are presented in Table 5B.3. On the basis of these results, Gibbs free energy reaction profile diagram corresponding to the ligand exchange reaction of **IIa** computed in the gas and solvent phase are shown in Fig.5B.3 and 5B.4. The activation free energy for the water exchange reaction of monoaqua

ruthenium(III) complex with histidine and cysteine are 24.41kcal mol^{-1} and 34.52 kcal mol^{-1}, respectively (Fig. 5B.3), indicating that **IIa** prefer to substitute aqua ligand with histidine rather than cysteine. The corresponding activation free energy values in the solvent phase are observed to be 21.24 and 32.94 kcal mol^{-1} which is slightly lower than the gas phase values (Fig. 5B.4). Similar activation free energy for **IIa** binding to histidine is reported by Fu and his coworkers on studying the binding mechanism of ruthenium(II) complex with amino acid residue (ΔG^{*}_{his} =22.63 kcal mol^{-1} (in gas phase), ΔG^{*}_{his} = 22.91 kcal mol^{-1} (in aqueous phase).[36] Lower activation free energy in aqueous medium (solvent) is obtained because of solvation of intermediates and transition states

Table 5B.3 Total relative energy (E_{tot}), relative enthalpy (ΔH) and free energy (ΔG) values of **IIa** with histidine and cysteine calculated at BLYP/DNP level. Energy values are in kcal mol^{-1}.

	Monoaqua			Monoaqua		
	R1	**TS1**	**P1**	**R2**	**TS2**	**P2**
E_{tot}	0	24.58(23.82)	1.88(0.38)	0	48.95(21.34)	1.26(1.88)
ΔH	0	22.21(19.04)	-1.33(-2.27)	0	21.22(19.64)	-0.77(-3.56)
ΔG	0	24.41(21.24)	2.04(1.00)	0	34.52(32.94)	-9.47(-12.26)
G_{solv}	0.93	-2.24	-0.005	3.33	1.75	0.54

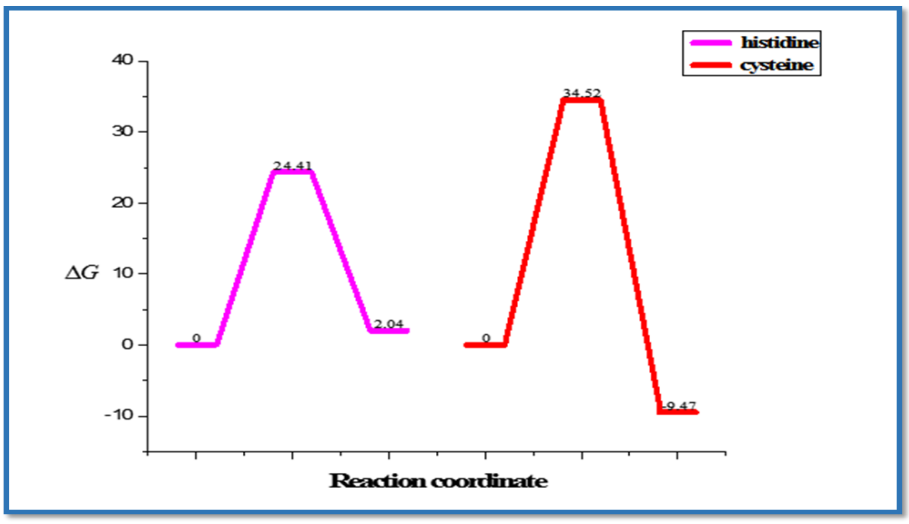

Fig. 5B.3 Free energy profile diagram of the monoaqua ruthenium(III) complex **IIa** binding to the histidine and cysteine in the gas phase calculated at BLYP/DNP level.

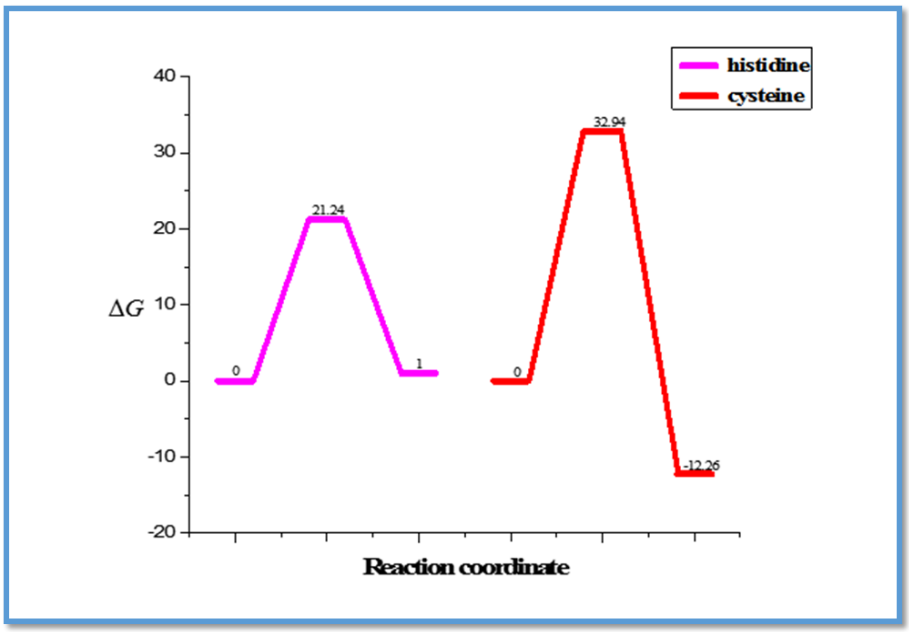

Fig. 5B.4 Free energy profile diagram of monoaqua ruthenium(III) complex **IIa** binding to the histidine and cysteine in the solvent phase calculated at BLYP/DNP level.

Solvation stabilized the activated complex to a greater extent by lowering the energy of the reactant as well as the transition state and hence speeds up the substitution reaction in aqueous medium. Therefore, ligand exchange reaction of **IIa** with histidine and cysteine occurs much more easily in the solvent medium as compared to gas medium. The observation of preferential binding of ruthenium complex with histidine is in agreement with the experimental results reported by Casini *et. al*., Vergara *et. al*. and Liu *et. al*. In their studies they presented the complete substitution of ligands of NAMI-A and its derivative with protein N-donor residues such as histidine, asparagine aspartic acid etc.[37-39] Furthermore, it has been observed from Table 5B.3 that in both the gas and solvent phases the enthalpy change (ΔH) acquired by the water exchange reaction of monoaqua complex with histidine and cysteine are ΔH_{his} = -1.33 kcal mol^{-1} (gas medium), ΔH_{his} = -2.27 kcal mol^{-1} (aquous medium) ΔH_{cys} = -0.77 kcal mol^{-1} (gas medium) and ΔH_{cys} = -3.56 kcal mol^{-1}(aquous medium). Negative value of ΔH implies that the ligand exchange reaction of monoaqua complex with histidine and cysteine are exothermic and hence, thermodynamically favorable.

Diaqua complex binding to histidine and cysteine

ΔH , ΔG and G_{solv} at 298.15K of all the stationary points of water exchange reaction of diaqua ruthenium complex **IIb** with histidine and cysteine in gas as well as in solvent phases are presented in Table 5B.4. The Gibbs free energy profile diagram for the ligand exchange reaction of **IIb** with histidine and cysteine in both the phases is shown in Fig. 5B.5 and 5B.6. From the free energy diagram reported in Fig. 5B.5 and 5B.6, it is noticed that the activation free energy values for the water exchange reaction of diaqua complex with protein residues in the aqueous medium (ΔG^{*}_{his} = 32.88 kcal mol^{-1}, ΔG^{*}_{cys} = 21.15 kcal mol^{-1}) are found to be lower than those in the gas phase (ΔG^{*}_{his} = 34.54 kcal mol^{-1}, ΔG^{*}_{cys} = 25.45 kcal mol^{-1}). Solvation lowers the activation energy in aqueous medium and makes the substitution reaction more feasible in aqueous medium than gas medium. These results clearly indicate that **IIb** can bind to histidine and cysteine much more easily in aqueous medium. The activation free energy value in aqueous medium for water exchange reaction of diaqua complex with cysteine is found to be closer to the experimental value of NAMI-A-cysteine binding (18.83 kcal mol^{-1}).[40] Our computed results show that mainly the diaqua form of ruthenium(III) complex prefer to bind cysteine residue. It is seen from Table 5B.4 that the activation enthalpy for the water substitution reaction of **IIb** with histidine and cysteine in solvent phase is observed to be 20.43 and 15.42 kcal mol^{-1} and the reaction is exothermic by 2.42 and 1.39 kcal mol^{-1}, respectively.

Table 5B. 4 Total relative energy (E_{tot}), relative enthalpy (ΔH) and free energy (ΔG) values of diaqua ruthenium(III) complex **IIb** with His and Cys calculated at BLYP/DNP level. Energy values are in kcalmol^{-1} .Solvent phase values are in parenthesis

		Diaqua			Diaqua	
	R1$^{/}$	**TS1**$^{/}$	**P1**$^{/}$	**R2**$^{/}$	**TS2**$^{/}$	**P2**$^{/}$
E_{tot}	0	34.51(30.87)	-7.22(-4.64)	0	29.50(25.73)	-5.02(0.19)
ΔH	0	22.09(20.43)	-0.82(-2.42)	0	19.68(15.42)	0.30(-1.39)
ΔG	0	34.54(32.88)	-7.21(-4.64)	0	25.45(21.15)	0.17(-0.84)
G_{solv}	0.90	-0.76	-0.70	1.18	-2.13	-0.51

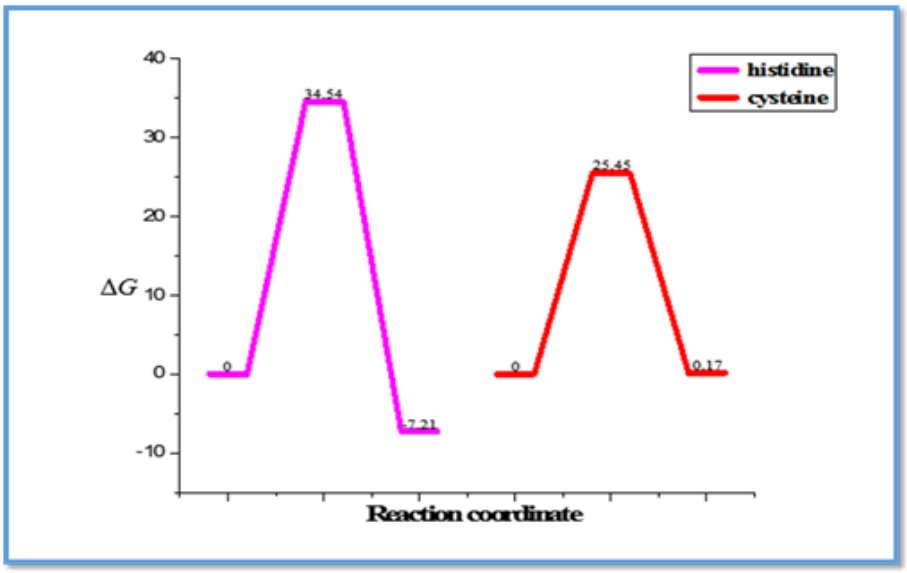

Fig. 5B.5 Free energy profile diagram of diaqua ruthenium(III) complex **IIb** binding to the histidine and cysteine in the gas phase calculated at BLYP/DNP level.

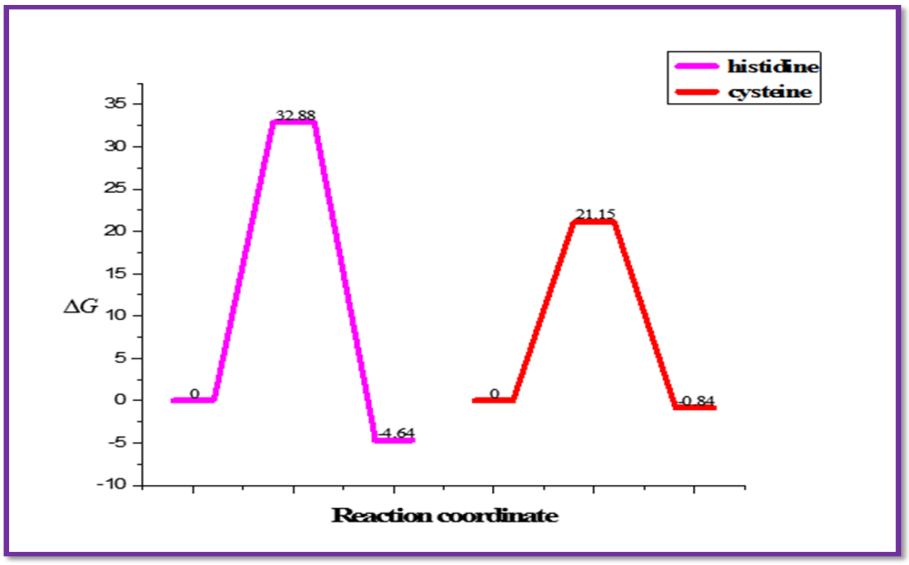

Fig. 5B.6 Free energy profile diagram of diaqua ruthenium(III) complex **IIb** binding to the histidine and cysteine in the solvent phase calculated at BLYP/DNP level.

5B.3.3 Kinetic analysis

The rate constant values for the ligand exchange reaction of **IIa** and **IIb** with histidine and cysteine in gas as well as in solvent phases are calculated by using Eyring equation via activation free energy values are presented in Table 5B.5. The calculated rate constant values for the monoaqua ruthenium complex binding to histidine and cysteine in solvent phase are $k_{his} = 1.67 \times 10^{-3}$ s^{-1} and $k_{cys} = 4.44 \times 10^{-12}$ s^{-1},

respectively, while the corresponding rate constant values for diaqua complex are k'_{his} = 4.91×10^{-12} s^{-1} and k'_{cys} =1.97×10^{-3} s^{-1}. Higher rate constant value in solvent phase compared to the gas phase (Table 5B.5) shows the importance of solvent effect on the binding interaction of ruthenium(III) complexes towards protein residue. Higher values of rate constant, higher will be the binding affinity of ruthenium (III) complex towards histidine and cysteine. Thus, the calculated results reveal that ligand exchange reaction of ruthenium(III) complexes with protein residues take place more easily in solvent medium compared to gas medium.

Table 5B. 5 Rate constant values for the substitution reaction of **IIa** and **IIb** with histidine and cysteine. Solvent phase values are presented in parenthesis

Rate constant(s^{-1})	**IIa**		**IIb**	
	k_{his}	k_{cys}	k'_{his}	k'_{cys}
K	7.97×10^{-6}	3.08×10^{-13}	2.99×10^{-13}	0.001×10^{-3}
	(1.67×10^{-3})	(4.44×10^{-12})	(4.91×10^{-12})	(1.97×10^{-3})

5B.4 Conclusion

In this present work, we have computationally investigated the binding mechanism of monoaqua ruthenium(III) complex [*trans*-$RuCl_3(H_2O)$(2H-indazole)(dmso-S)] (**IIa**) and diaquated complex [*trans*-$RuCl_2(H_2O)_2$(2H-indazole)(dmso-S)]$^{+1}$ (**IIb**) with histidine and cysteine using the density functional theory at BLYP/DNP level. The activation free energy for aqua ligand substitution reaction of monoaqua ruthenium complex(III) with histidine (21.24 kcal mol^{-1}) is found to be lower than the corresponding value with cysteine (32.94 kcal mol^{-1}), hence the reaction with histidine is faster which is attested by the calculated rate constant values. Again, the activation free energy for the water exchange reaction of diaqua complex with histidine and cysteine is found to be 32.88 kcal mol^{-1} and 21.15 kcal mol^{-1}, respectively, in solvent phase. The ligand exchange reaction of monoaqua ruthenium complex with histidine is found to be easier than the diaqua ruthenium complex, while the opposite result is obtained with cysteine. Our calculated results also reveal that the incorporation of solvent on the ligand exchange reaction with protein residue has a profound effect.

References

1. A. Martinez, *Amino Acids*, 1995, **9**, 285–292.
2. K. Uchida, *Amino Acids*, 2003, **25**, 249–257.
3. M. Remko, D. Fitz, B. M. Rode, *Amino Acids*, 2010, **39**, 1309–1319.
4. F. Li, D. Fitz, D. G. Fraser, B. M. Rode, *Amino Acids*, 2010, **38**, 287–294.
5. F. Schneider, *Angew. Chem., Int. Ed. Engl*., 1978, **17**, 583-592.
6. R. J. Sundberg, R. B. Martin, *Chem. Rev*., 1974, **74**, 471-517.
7. M. Agnieszka, K. W. Janina, K. K. Katarzyna, *J. Mol. Struc*., 2003, **655**, 397–403.
8. M. B. Smith, J. March, *March's Advanced Organic Chemistry: Reactions, Mechanisms, and* Structure, 6th edition, New York: Wiley-Interscience, 2007.
9. J. Luo, J. F. Wishart, S. S. Isied, *J. Am. Chem. Soc*., 1998, **120**, 12970-12971.
10. S. S. Isied, G. Worosila, S. J. Atherton, *J. Am. Chem. Soc*., 1982, **104**, 7659-7661.
11. S. S. Isied, C. Kuehn, G. Worosila, *J. Am. Chem. Soc*., 1984, **106**, 1722-1726.
12. J. Sun, J. F. Wishart, M. B. Gardineer, M. P. Cho, S. S. Isied, *Inorg. Chem*., 1995, **34**, 3301-3309.
13. J. F. Wishart, J. Sun, M. Cho, C. Su, S. S. Isied, *J. Phys. Chem. B*, 1997, **101**, 687-693.
14. B. D. Durham, L. P. Pan, S. Hahm, J. Long, F. Millett, *In Electron Transfer in Biology and the Solid State*, M. K. Johnson, R. B. King, D. M. Kurtz, C. Kutal, M. L. Norton, R. A. Scott, Eds.; Advances in Chemistry Series 226, American Chemical Society: Washington, DC, 1990, pp. 180.
15. P. K. Chattaraj, *J. Phys. Chem. A*, 2001,**105**, 511–513.
16. R. G. Parr, R. G. Pearson, *J. Am. Chem. Soc*., 1983,**105**, 7512–7516.
17. C. M. Riley, L. A. Sternson, A. J. Repta, S. A. Slyter, *Anal. Biochem*., 1983, **130**, 203–214.
18. D. H. Kim, J. K. Kundu, Y. J. Surh, *Mol.Carcinog*., 2011, **50**, 222-234.
19. A. Sarasin, G. Giglia-Mari, *Exp. Dermatology*, 2002, **11**, 44-47.
20. R. J. Osborne, G. R. Merlo, T. Mitsudomi, T. Venesio, D. S. Liscia, A. P. M. Cappa, I. Chiba, T. Takahashi, M. M. Nau, R. Callahan, J. D. Minna, *Cancer Res*., 1991, **51**, 6194-6198.

21. M. Hollstein, D. Sidransky, B. Vogelstein, C. C. Harris, *Science*, 1991, **253**, 49-53.

22. C. C. Harris, *J. National Cancer Inst*., 1996, **88**, 1442-1455.

23. R. Rainwater, D. Parks, M. E. Anderson, P. Tegtmeyer, K. Mann, *Mol. Cell. Biol*., 1995, **15**, 3892-3903.

24. H. Jung, H. A. Seong, H. Ha, *J.Biol. Chem*., 2008, **283**, 20383-20396.

25. B. Delly, *J. Chem. Phys*., 1990, **92**, 508-517.

26. A. D. Becke, *Phys. Rev. A*, 1998, **38**, 3098-3100.

27. C. Lee, W. Yang, R. G. Parr, *Phys. Rev. B*, 1998, **37**, 785-789.

28. C. W. Bock, M. Trachtman, *J. Phys. Chem*., 1994, **98**, 95.

29. M. S. Gordon, *Chem. Phys. Lett*., 1980, **76**, 163-168.

30. W. J. Hehre, R. Ditchfield, J. A. Pople, *J. Chem. Phys.*, 1972, **56**, 2257-2261.

31. N. Govind, M. Petersen, G. Gitzgerald, D. King-Smith, J. J. Andzelm, *Comput. Mater. Sci*., 2003, **28**, 250−258.

32. Materials Studio Accelrys Inc., San Diego CA, USA, 2006.

33. J. Andzelm, C. Koelmel, A. Klamt, *J. Chem. Phys*., 1995, **103**, 9312-9320.

34. K. A. Connors, In: *Chemical Kinetics-The Study of Reaction Rate in Solution*, Wiley, New York, 1990.

35. J. Chen, L. Chen, L. Siyan, K. Zheng, L. Ji, *J. Phys. Chem. B*, 2007, **111**, 7862-7869.

36. Q. Fu, L. Zhou, J. Li, S*truct. Chem*., 2012, **23**, 1931–1940.

37. A. Casini, G. Mastrobouni, M. Terenghi, C. Gabbiani, E. Monzani, G. Moneti, L.Casella, L. Monzani, G. Moneti, L. Casella, L. Messori, *J. Biol. Inorg. Chem*., 2007, **12**, 1107-1117.

38. A. Vergara, G. D'Errico, D. Montesarchio, G. Mangiapia, L. Paduan, A. Merlino, *Inorg. Chem*., 2013, **52**, 4157-4159.

39. M. Liu, Z. J. Lim, Y. Y. Gwee, A. Levina, P. A. Lay, *Angew. Chem. Int. Ed*., 2010, **49**, 1661 –1664.

40. R. A. Adigun, PhD Thesis Portland State University, 2012.

QUANTUM CHEMICAL STUDIES ON DETAIL MECHANISM OF NITROSYLATION OF RUTHENIUM(III) COMPLEX-HSA ADDUCT

5C.1 Introduction

Nitric oxide (NO) produced by a number of nitric oxide synthase (NOS) enzymes from L-arginine in the body[1], is an important signaling molecule involves in the regulation of different physiological processes such as neural transmission, regulation of cardiovascular function, apoptosis and immune defense in mammels.[2] On the other hand, being a free radical, nitric oxide is highly toxic to the cells. NO exhibits an important role in maintaining the vasodilatory tone of tumors by regulating tumor blood flow[3] and closely linked to the growth and progression of several human tumors.[4-6] It also acts as an active mediator for the tumor angiogenesis.[7,8] Systematic inhibition of nitric oxide synthase (NOS) or inactivation of free NO in tumors through the availability of drug molecules has been demonstrated as a new alternative therapeutic approach towards inhibiting tumor angiogenesis.[9] Clinically established ruthenium complex, NAMI-A is reported to have an angiogenesis inhibitory activity.[10,11] Because of the involvement of nitric oxide in contributing many tumor progression as well as its ability to interact ruthenium complexes[12], a theory has been proposed which says that interference of NAMI-A with nitric oxide may be one of the possible routes for its antimetastatic activity.[13,14]Increasing evidences in the literature have shown that NAMI-A, KP1339 (Na[*trans*-RuCl4(Ind)2], Ind – indazole)[15-17] and Ru(EDTA) complexes capable of inhibiting NO-dependent angiogenesis by capturing NO *in vivo* and *in vitro* without affecting the intracellular mechanism involved in proliferation.[18,19]

NO interacts with NAMI-A and other ruthenium(III) complexes in a linear fashion to give ruthenium nitrosyl complexes which is formally described as [Ru^{II}—NO^{+}].[20] Change in the oxidation state of the ruthenium(III) occurring upon NO binding is characterized by an weak absorption band at around 500 nm and are substantially different from parent ruthenium(III) complexes characterized by relatively strong ligand-to-metal charge transfer bands.[21] Along with the antimetastatic and antiangiogenesis activities of ruthenium(III) complexes, they have also investigated the nitric oxide scavengers.[22,23] These complexes exhibit pharmacological activity *in vitro* and in a number of *in vivo* models for a variety of diseases including cancer.[24]

The NO scavengers will be effective if they will meet the criteria such as fast NO reaction kinetics, activity and stability *in vitro* and *in vivo* biological systems, low toxicity and rapid clearance from the organism.[25]

Until now, numbers of experimental reports on the nitrosylation reaction of ruthenium based drugs have been performed but to the best of our knowledge only a few computational studies have been performed at the molecular level. The aim of our present study is to investigate the NO scavenging capability of the clinically established ruthenium(III) complex, at the molecular level. We have studied the interaction mechanism of ruthenium(III) complex -HSA (HSA= human serum albumin) with NO, because NAMI-A binds to the plasma proteins after intravenous administration. The ruthenium(III) complex -HSA adduct, **Ia-HSA** has been taken from our studies conducted on ruthenium(III) complex-protein interaction which is discussed in chapter 5A. Hydrolysis of **Ia-HSA** adduct has been performed prior to reaction with NO in which one of the Cl^- ligand is substituted with a water ligand. Water being a labile substituent in the **Ia-HSA** adduct can easily exchange with various ligands.

5C.2 Computational Details

Hydrolysis and nitrosylation reaction mechanisms of **Ia-HSA** adduct have been carried out using the density functional theory, employing the Gaussian 09 program package.[26] The gas phase optimization of reactants, products and transition states without imposing any symmetry constraint have been done using the B3LYP[27] exchange-correlation functional with 6-31G(d,p)[28] and LANL2DZ[29] basis sets. The effective core potential basis set LANL2DZ for ruthenium atom while 6-31G(d, p) basis set for all other atoms are used. A vibrational analysis has been performed at the same level of theory, to ensure that optimized structures are minima or transition states and to estimate zero-point vibrational energies and thermal and entropic corrections. The transition states are also confirmed by intrinsic reaction coordinate (IRC) calculations.[30,31] In order to obtain accurate energies for the reaction surfaces, single-point energies are calculated on optimized structures using a higher basis set of LanL2DZ (on Ru atom), 6-311+G(d, p) (on H, C, N, O atoms) and 6-311+G(3d) (on Cl, S atoms) in vacuo.[32,33] Single point energies are also evaluated using implicit solvation model CPCM.[34]

Free energies, enthalpies and solvation free energies are computed by using the following equations:[35]

$$G_{solv} = G_{solvent} - G_{gas}$$

$$H(aq) = E_{ZPE}(g) + G_{solv} + H_{therm}\ (g)$$

$$G(aq) = E_{ZPE}(g) + G_{solv} + G_{therm}(g)$$

Where G_{solv} is the solvation energy, $G_{solvent}$ is the Gibbs free energy in solvent medium, G_{gas} is the Gibbs free energy in gas phase, $H(aq)$ is the enthalpy and $G(aq)$ is the Gibbs free energy in aqueous medium, $H_{therm}(g)$ is the thermal correction to enthalpy and $G_{therm}(g)$ is the thermal correction to Gibbs free energy in the gas phase.

Activation free energies (free energy difference between the transition state and original state) is used to calculate rate constants for all the substitution reactions via transition state theory formalism[36] proposed by Eyring as

$$k(T) = \frac{K_B T}{h} e^{-\Delta G^{\neq}/RT}$$

Where K_B is the Baltzmann constant, T is the absolute temperature and $\Delta G^{\neq}$ is the activation free energy.

Reduction potentials (E_m) at standard conditions are obtained from the following equation:

$$E_m = \Delta G \diagup nF$$

F is the Faraday constant (F=96485C), E_m is the reduction potential, n is the number of electrons take part in the redox reaction.

5C.3 Results and Discussion

5C.3.1 Structural characteristics

Fully optimized structures of all the species involved in the hydrolysis of **Ia-HSA** adduct calculated at B3LYP(LANL2DZ+6-31G(d,p)) level is presented in Fig. 5C.1 and significant geometrical parameters are listed in Tables 5C.1. From Fig. 5C.1 and Table 5C.1, it is noticed that in the reactant **R**, **Ia** retains its pseudooctahedral geometry with three equatorial chloro ligands, one equatorial histidyl residue and two axial ligands namely DMSO and imidazole group. The Ru—Cl1, Ru—Cl2, Ru—Cl3,

Ru—N_{his} bond distances are found to be 2.42, 2.40, 2.38 and 2.18 Å whereas Ru—N and Ru—S bond lengths are calculated to be 2.11 and 2.43 Å, respectively. The bond angles Cl1—Ru— N_{His} and Cl2—Ru— N_{His} are observed to be 85.7^0 and 88.1°, respectively. Observed deviation of bond angle from 90^0 reveals hexa-coordinated distorted octahedral geometry of **R**. Table 5C.1 suggests that DFT computed bond distances are found to be slightly longer than the X-ray crystallographic data.[37] These differences in bond distances may be due to the systematic error caused by the computational methods and environment factors.[38] It is also observed that **Ia** forms a hydrogen bonding between DMSO oxygen atom and one of the hydrogen atoms of glutamine side chain (2.03 Å). Presence of hydrogen bonding gives additional stability to **R**. In the intermediate **I-1**, the water molecule approaches the reaction center via hydrogen bonding with the adjacent Cl^- ligand ($HOH^{\cdots}Cl$) at a distance of about 2.37 Å. The transition state found for the hydrolysis step of **Ia-HSA** adduct is confirmed by presence of an imaginary frequency and having pentagonal bipyramidal arrangement. The Ru—O(wat) bond distance is reduces from 4.96 Å in **I-1** to 2.84 Å in TS while, the Ru-Cl2 distance increases from 2.42 to 2.86 Å, hence, it follows an interchange dissociative mechanism. The structure of intermediate **I-2**, is observed to be pseudo-octahedral in which Cl^- ligand is completely exchanged by aquo ligand and forms a bond with Ru^{3+} ion at distance of 2.14 Å. Again the leaving Cl^- ligand forms intermolecular hydrogen bonding with H atom of the coordinated water molecule at distance of 1.77 Å. The product **P** attains a pseudooctahedral configuration, where Cl^- ligand is completely removed from the system, and the coordinated water molecule forms a hydrogen bond with O atom of histidyl residue at distance of 1.83 Å.

Fig. 5C.2 displays the optimized stationary point for nitrosylation of **P** (hydrolysed product of **Ia-HSA** adduct) with nitric oxide and the important geometrical parameters are summarized in Table 5C.2. In the optimized intermediate structure of nitrosylation **I-3**, the hydrogen atom of coordinated water molecule forms an interconnected hydrogen bonding interaction with the oxygen atom of histidyl residue at 1.87 Å. In **I-3**, the bond distance between nitrogen atom of NO molecule with ruthenium ion is found to be 3.89 Å. Transition state, **TS1** a heptacoordinate geometry is confirmed by the presence of one imaginary frequency.

Table 5C.1 Optimized geometric parameters (bond length in Å and bond angles in ^{0}) of all the stationary points in chloride exchange reaction of **Ia-HSA** adduct with water at the level of B3LYP/(LANL2DZ+6-31G(d,p) in gas phase.

Parameters	**R**	**I-1**	**TS**	**I-2**	**P**
Ru—N_{his}	2.18	2.18	2.16	2.13	2.15
Ru—Cl2	2.42	2.42	2.86	4.14	
Ru—Cl3	2.38	2.38	2.44	2.39	2.38
Ru—Cl4	2.40	2.41	2.38	2.36	2.33
Ru—S	2.43	2.44	2.51	2.49	2.45
Ru—N	2.11	2.11	2.13	2.10	2.12
Ru—O(wat)		4.96	2.84	2.14	2.23
H1—O(wat)		2.46			
Cl2—H(wat)		2.37	2.07	1.77	
O(his)—H(wat)					1.83
DMSO—H_{Gln}	2.03	2.02	1.99	2.02	2.15
N1—Ru—S1	172.8	172.5	166.9	171.7	173.6
N_{his}—Ru—Cl2	88.1	87.0	70.3	60.5	
Cl2—Ru—Cl3	92.8	93.1	115.2	97.0	
Cl3—Ru—Cl4	93.4	93.8	91.0		96.4
Cl4—Ru—N_{his}	85.7	86.1	83.9	89.9	88.4
O(wat)—Ru—Cl3			70.6	85.7	81.9
O(wat)—Ru—N_{his}				87.5	91.6

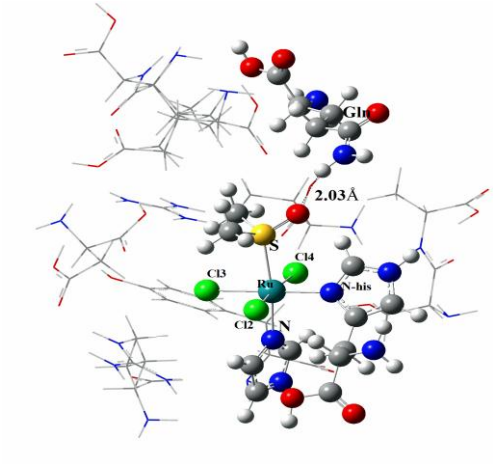

R

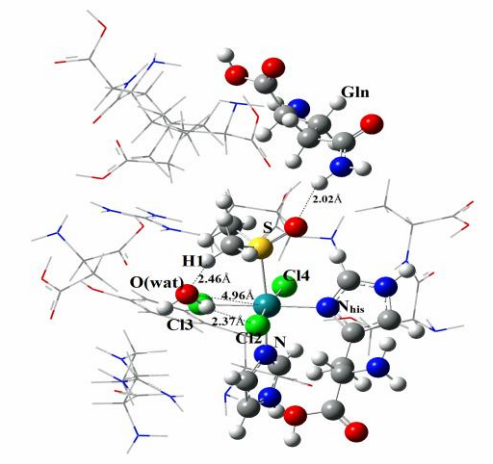

I-1

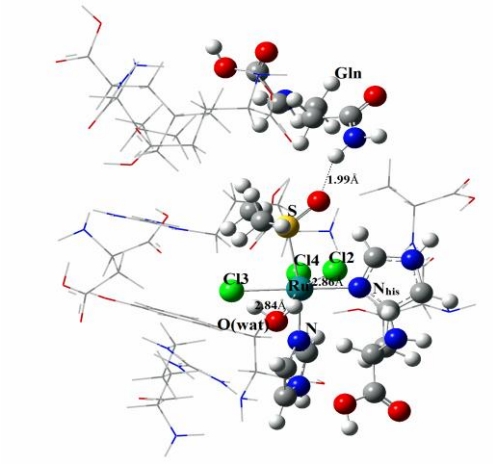

TS

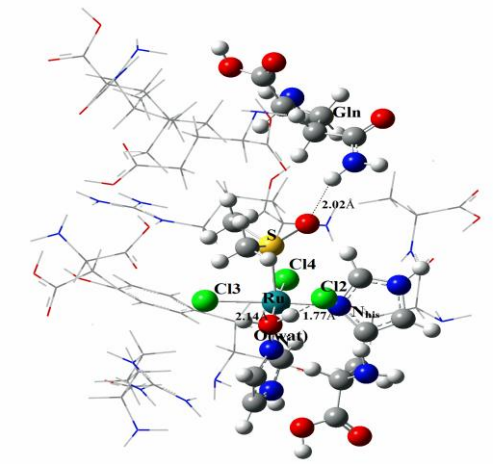

I-2

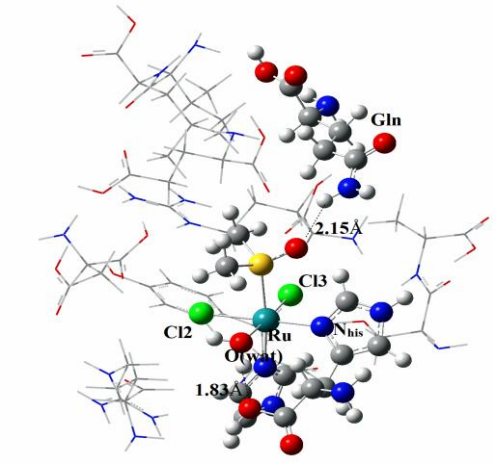

P

Fig. 5C.1 Optimized structures for the species involved in hydrolysis reaction of **Ia-HSA** adduct calculated at B3LYP/ (LanL2DZ and 6-31G(d,p)) level.

In **TS1**, the entering NO molecule approaches the reaction center where Ru—NO distance decreases from 3.89 to 3.80 Å, while, the leaving water ligand moves from the reaction center with Ru—O distance increases from 2.25 to 5.96 Å, indicating a dissociative character of the transition state. In **I-4** intermediate, the incoming NO group (Ru—NO=1.78Å) replaces the water molecule (Ru—H_2O =5.01 Å) and coordinated with the ruthenium center. Thus the nitrosylation product **P1** has a pseudooctahedral geometry, where aquo ligand is completely removed from the system by NO. NO strongly binds in the adduct **P1**, resulting in the reduction of the Ru^{3+} to Ru^{2+} ion to form a linear Ru^{2+}—NO^{+} bond.

NO, when gets coordinated with the Ru^{3+}, the unpaired electron originating from NO transfers to the ruthenium ion, making the spin coupled linear Ru^{2+}—NO^{+} adduct **P1**, in agreement with experimental studies by Oszajca *et. al.*[20] Reduction potential for **P1** is observed to be -2.32V, is closer to the experimental reduction potential.[20] Ru^{2+} ion with d^6 electronic configuration exhibits lesser stability than Ru^{3+} since distribution of electronic charge is not uniform and exchange energy of electrons are less, hence more reactive. Thus NO interaction plays an important role in describing the antimetastatic activity of **Ia**. Probable mode of action involved in the NO interaction to **Ia-HSA** is as follows:[38]

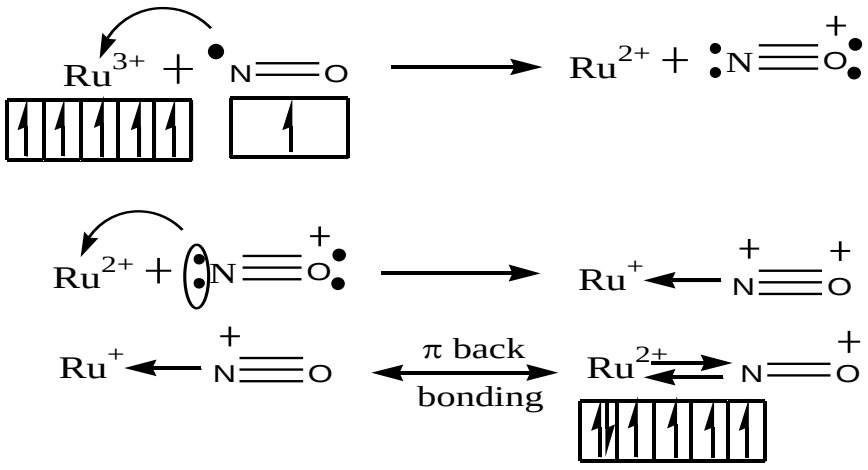

Table 5C.2 Optimized geometric parameters (bond length in Å and bond angles in ^{0}) of all the stationary points in water exchange reaction of **Ia-HSA** adduct with nitric oxide at the level of B3LYP/(LANL2DZ+6-31G(d,p) in gas phase

Parameters	**I-3**	**TS1**	**I-4**	**P1**
Ru—N_{his}	2.15	2.12	2.17	2.17
Ru—Cl3	2.47	2.33	2.42	2.42
Ru—Cl4	2.42	2.29	2.37	2.36
Ru—S	2.26	2.46	2.48	2.49
Ru—N	2.11	2.11	2.13	2.12
O(his)—H(wat)	1.86			
Ru—O(wat)	2.25	5.96	5.03	
Ru—N(NO)	3.89	3.80	1.78	1.78
DMSO—H_{Gln}	2.55	2.11	2.19	2.22
H1—O(wat)		2.78	2.63	
N1—Ru—S1	169.5	174.0	171.4	171.5
N_{his}—Ru—NO		101.1	96.4	97.5
NO—Ru—Cl3		65.6	88.3	87.2
Cl3—Ru—Cl4	94.8	101.2	89.0	88.8
Cl4—Ru—N_{his}	86.9	91.6	86.2	86.5
N_{his}—Ru—O(wat)	100.1			
O(wat)—Ru—Cl3	78.1			

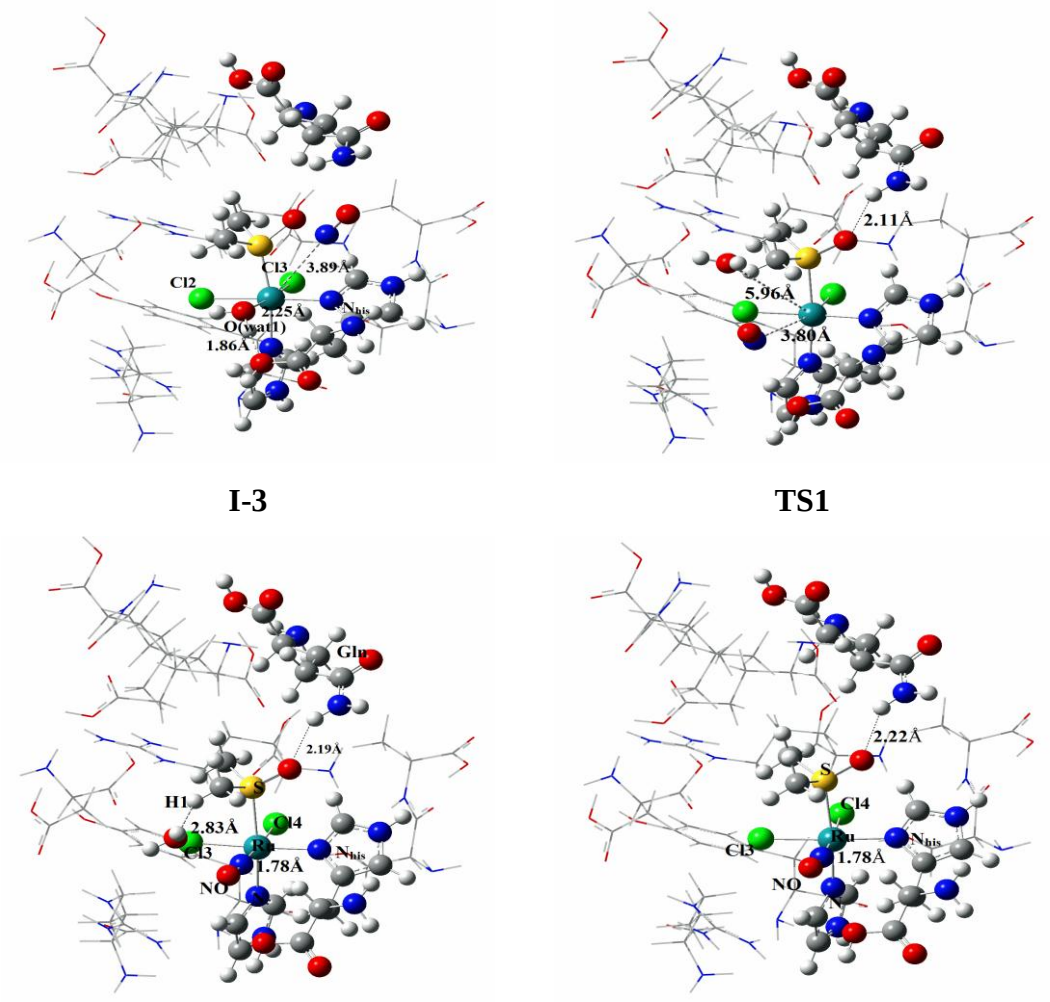

Fig. 5C.2 Optimized structures for the species involved in nitrosylation reaction of hydrolyzed **Ia-HSA** adduct calculated at B3LYP/ (LanL2DZ and 6-31G(d,p)) level.

5C.3.2 Energy profiles

Change of enthalpies, Gibbs free energies, solvation energies, thermal corrections to the enthalpies, thermal contribution to Gibbs free energies of all the stationary points for the hydrolysis of **Ia-HSA** adduct at 298.15K in the gas and solvent phases calculated at DFT-B3LYP level are presented in Table 5C.3. On the basis of these results, Gibbs free energies corresponding to the hydrolysis process of **Ia-HSA** adduct computed in the gas and solvent phases are provided in the form of a reaction profile diagram in Fig. 5C.3 and 5C.4. It can be noted from Fig. 5C.3 that the activation free energy for the hydrolysis of **Ia-HSA** adduct is found to be 33.77 kcal mol^{-1}. Incorporation of solvent (water) effect by using CPCM model lowers the activation free energy for this hydrolysis reaction and is found to be 24.97 kcal mol^{-1} (Fig. 5C.4),

which is in agreement with the experimental activation energy value reported by Bouma *et. al.*[39] The decrease in activation free energy in aqueous medium may be due to the fact that in aqueous medium, all the reactants, intermediates and product species remain in the solvated state. Solvation lowers the energy of the species and makes the reaction easier.

Table 5C.3 Total ZPE ($E_{tot/ZPE}$), solvation energies (G_{solv}), thermal contributions to enthalpies (H_{therm}), thermal contribution to Gibbs free energies (G_{therm}), change of enthalpies (ΔH) and change of Gibbs free energies (ΔG) 298.15 K for the species involved in hydrolysis process of **Ia-HSA** adduct. Energy values are in kcal mol^{-1}, entropy values are in cal k^{-1} mol^{-1} and rate constant value is in s^{-1}. Solvent phase values are in parenthesis.

Species	$E_{tot/ZPE}$	G_{solv}	H_{therm}	G_{therm}	ΔH	ΔG	ΔS	k
I-1	0	-33.87	355.67	264.26	0	0	0	1.10×10^{-12}
								(3.09×10^{-6})
TS	31.38	-42.67	355.55	266.65	31.26	33.77	-8.44	
					(22.46)	(24.97)	(-0.61)	
I-2	-0.63	-38.28	354.97	265.75	-1.33	0.86	-7.36	
					(-5.74)	(-3.55)	(0.20)	

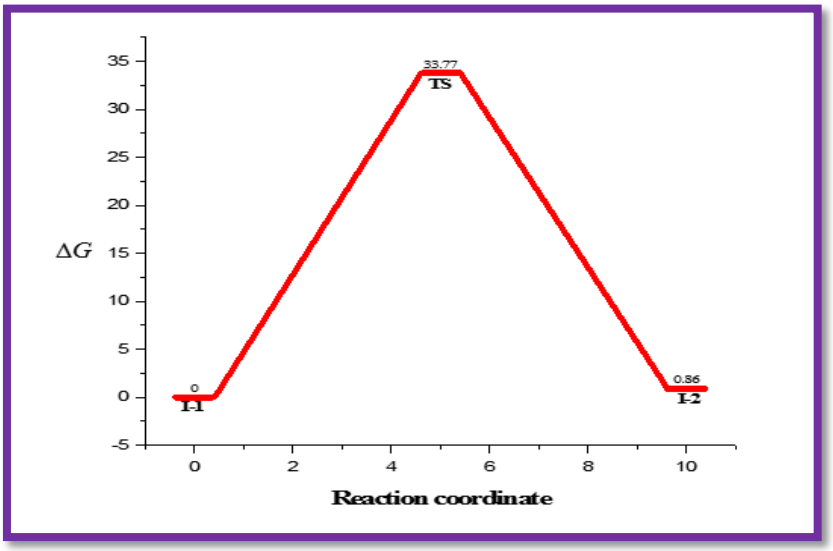

Fig. 5C.3 Free energy profile diagram of the hydrolysis step of **Ia-HSA** adduct in gas phase calculated at B3LYP/ (LanL2DZ and 6-31G(d,p)) level.

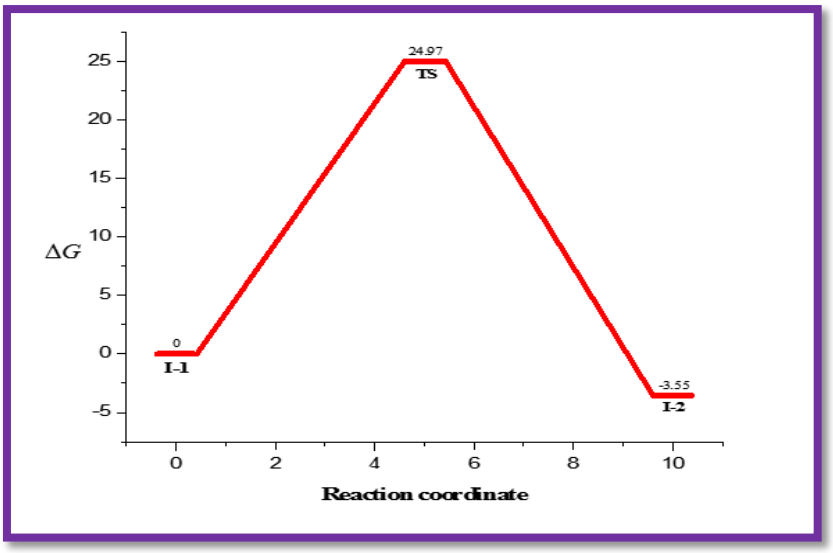

Fig. 5C.4 Free energy profile diagram of the hydrolysis step of **Ia-HSA** adduct in solvent phase calculated at B3LYP/ (LanL2DZ and 6-31G(d,p)) level.

Fig. 5C.5 presented the computed enthalpy profile for the hydrolysis reaction of **Ia-HSA** adduct in the solvent phase. It has been observed that activation enthalpy for the hydrolysis reaction in solvent phase is 22.46 kcal mol^{-1} in agreement with the experimental evidence.[39] Moreover, the hydrolysis reaction is predicted to be exothermic by 5.73 kcal mol^{-1} in solvent phase, as observed from Fig. 5C.5 indicating that the reaction is thermodynamically favored.

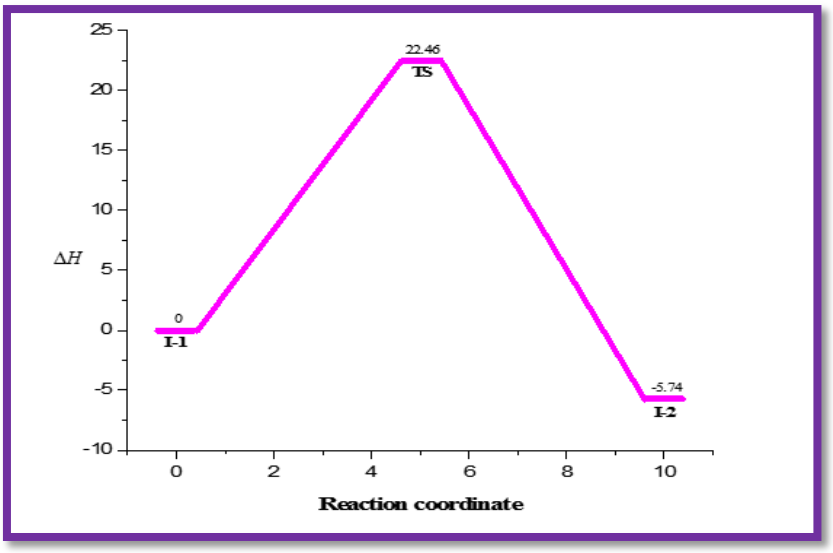

Fig. 5C.5 Enthalpy profile diagram of the hydrolysis step of **Ia-HSA** adduct in solvent phase calculated at B3LYP/ (LanL2DZ and 6-31G(d,p)) level.

Change of enthalpies, Gibbs free energies, solvation energies, thermal corrections to the enthalpies, thermal contribution to Gibbs free energies at 298.15K for all the stationary points of nitrosylation reaction of hydrolyzed **Ia-HSA** adduct in gas as well as solvent phases are presented in Table 5C.4.

Table 5C.4 Total ZPE ($E_{tot/ZPE}$), solvation energies (G_{solv}), thermal contributions to enthalpies (H_{therm}), thermal contribution to Gibbs free energies (G_{therm}), change of enthalpies (ΔH) and change of Gibbs free energies (ΔG) and rate constant at 298.15 K for the species involved in the nitrosylation reaction of hydrolyzed **Ia-HSA** adduct. Energy values are in kcal mol^{-1}, entropy values are in cal k^{-1} mol^{-1} and rate constant value is in s^{-1}. Solvent phase values are in parenthesis.

Species	$E_{tot/ZPE}$	G_{solv}	H_{therm}	G_{therm}	ΔH	ΔG	ΔS	k
I-3	0	-66.52	360.00	269.75	0	0	0	1.12×10^{2} (1.29×10^{6})
TS1	22.59	-73.42	358.76	263.16	21.35 (14.45)	16.01 (9.11)	4.40 (8.78)	
I-4	-38.27	-67.77	360.49	267.59	-37.78 (-39.03)	-40.43 (-41.66)	4.89 (13.90)	

Gibbs free energy diagram for the water exchange reaction of hydrolyzed **Ia-HSA** adduct with NO in the gas and solvent phases are shown in Fig. 5C.6 and 5C.7. Comparing the free energy diagram in Fig. 5C.6 and 5C.7, it is noticed that inclusion of solvent effect reduces the activation free energy from 16.01 kcal mol^{-1} to 9.11 kcal mol^{-1}. This decrease in activation energy in aqueous medium is due to solvation which solvates the reactants and intermediates through hydrogen bonding network. The hydrogen bonding network stabilized the solvated species to a greater extent by decreasing its energy, hence, enhances the stability of activated complex and makes the nitrosylation reaction more feasible in aqueous medium in comparison to gaseous medium. Fig. 5C.8 displays the enthalpy profile diagram for the water exchange reaction of hydrolyzed **Ia-HSA** adduct with nitric oxide in solvent medium. The

activation enthalpy value for this nitrosylation reaction is observed to be 14.45 kcal mol^{-1} and the reaction is exothermic by 39.03 kcal mol^{-1}.

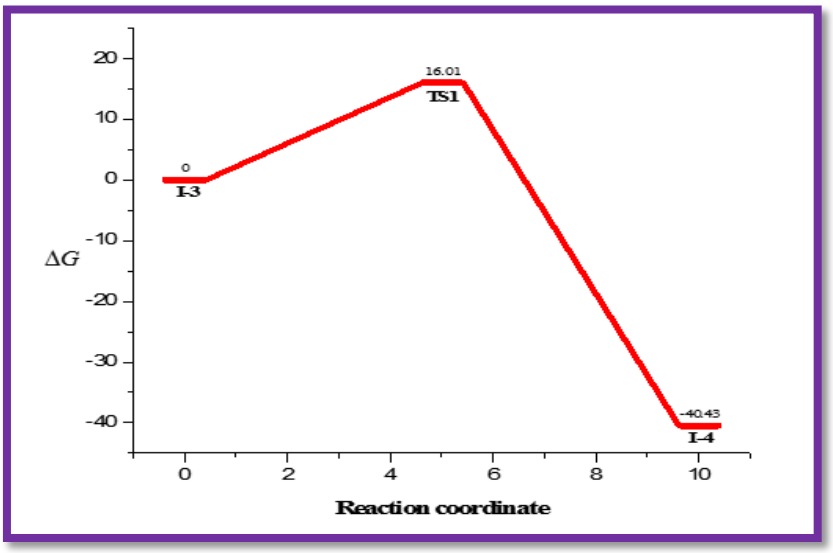

Fig. 5C.6 Free energy profile diagram of the nitrosylation step of **Ia-HSA** adduct in gas phase calculated at B3LYP/ (LanL2DZ and 6-31G(d,p)) level.

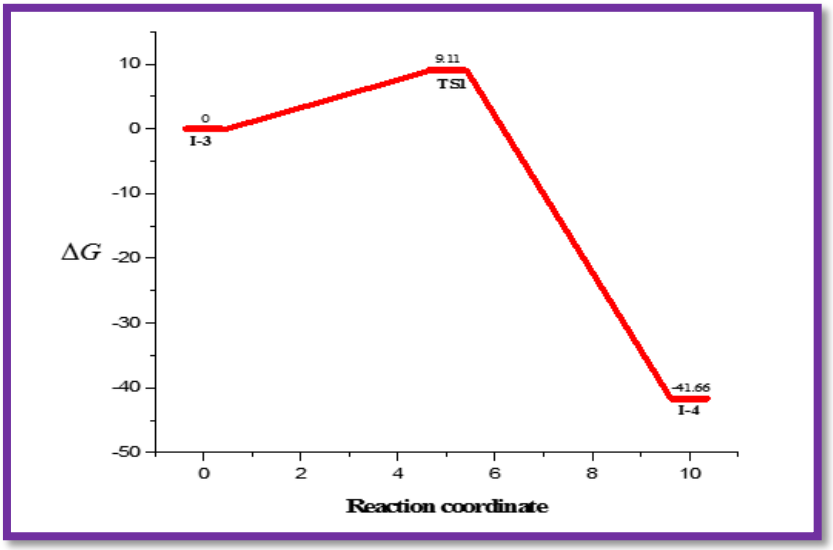

Fig. 5C.7 Free energy profile diagram of the nitrosylation step of **Ia-HSA** adduct in solvent phase calculated at B3LYP/ (LanL2DZ and 6-31G(d,p)) level

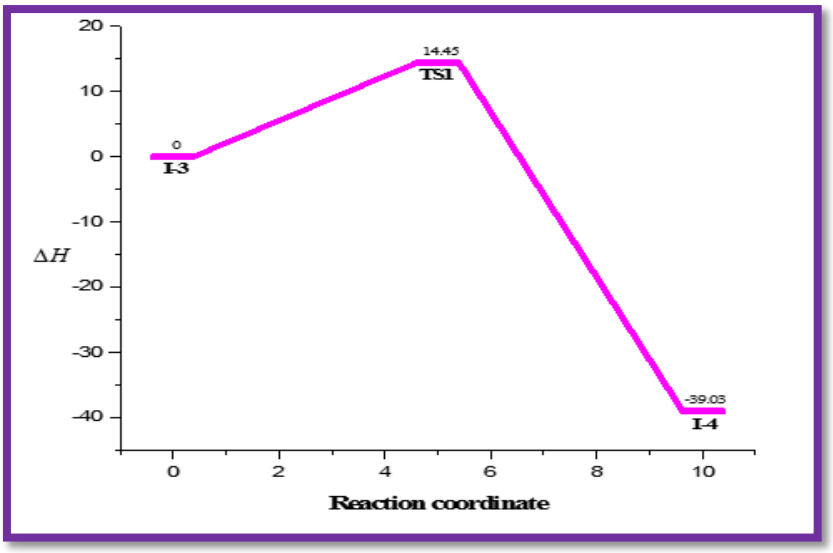

Fig. 5C.8 Enthalpy profile diagram of the nitrosylation step of **Ia-HSA** adduct in solvent phase calculated at B3LYP/ (LanL2DZ and 6-31G(d,p)) level.

5C.3.3 Kinetic analysis

The rate constant values for aquation and nitrosylation reaction of **Ia-HSA** adduct are calculated by using Eyring equation via activation free energy values and results are summarized in Table 5C.3 (hydrolysis reaction) and Table 5C.4 (nitrosylation reaction). The value obtained for the hydrolysis reaction of **Ia-HSA** adduct (k =3.09× 10^{-6} s^{-1}) in solvent phase is closer to the experimental values (5.58 × 10^{-6} s^{-1} in phosphate buffer (pH 7.4) when exposed to light).[40] Higher rate constant value in solvent phase compared to the gas phase (k =1.10× 10^{-12} s^{-1}) shows the importance of solvent effect on the hydrolysis reaction of **Ia-HSA** adduct. The rate constant value for water exchange reaction of **Ia-HSA** adduct with nitric oxide is observed to be k =1.29 × 10^{6} s^{-1} in aqueous phase while the gas phase value is k =1.12 × 10^{2} s^{-1}, revealing that the rate of nitrosylation reaction is much faster in aqueous phase. The rate constant values for NO binding to hydrolysed **Ia-HSA** adduct in solvent medium can be comparable with available literature of NO binding to ferric iron in microperoxidase.[41]

5C.4 Conclusion

We have computationally investigated the hydrolysis mechanism of **Ia-HSA** adduct using the DFT-B3LYP method. Hence, nitrosylation of hydrolyzed **Ia-HSA** adduct with nitric oxide is also performed in order to understand the antimetastatic property

of **Ia.** Our computed results reveal that the mechanism responsible for chloride exchange reaction in **Ia-HSA** adducts with water is an interchange dissociative mechanism, passing through a heptacoordinate transition state. Activation free energy and rate constant value for this reaction is found to be 24.97 kcal mol^{-1} and 3.09×10^{-6} s^{-1}, respectively in solvent phase, in agreement with experimental results. In the transition state of ligand exchange reaction of hydrolyzed form of **Ia-HSA** adduct with nitric oxide is obtained to be heptacoordinated geometry. Similar to hydrolysis of **Ia-HSA** adduct, nitrosylation also leads to lower activation free energy value in solvent medium (9.11 kcal mol^{-1}) than gas medium (16.01kcal mol^{-1}). The rate constant value for nitrosylation in solvent medium is 1.29×10^{6} s^{-1}, correlates well with experimental results and concern reaction is also found to be exothermic. These results reveal that the nitric oxide exchange reaction is fast and favorable. It is interesting to note that nitric oxide reduces ruthenium(III) to active ruthenium(II) with a reduction potential of -2.32V. Present work provides a detailed structural properties and energy profiles for the hydrolysis and nitrosylation mechanism of ruthenium(III) complex **Ia**, inside the protein environment which may contribute in understanding the antimetastatic activity of this drug as well as its NO scavenging ability.

References

1. R. B. Silverman, *Acc. Chem. Res.*, 2009, **42**, 439–445.
2. Y. C. Hou, A. Janczuk, P. G.Wang, 1999, **5**, 417–441.
3. D. Fukumura, F. Yuan, M. Endo, R. K. Jain, *Am. J. Pathol*., 1997, **150**, 713–725.
4. D .A. Wink, Y. Vodovotz, J. Laval, F. Lava, M. W. Dewhirst, J. B. Mitchell, *Cancerogenesis*., 1998, **19**, 711–721.
5. O. Gallo, E. Masini, L. Morbidelli, A. Franchi, I. Fini-Storchi, W. A. Vergari, M. Ziche, *J Natl. Cancer Inst*., 1998, **90**, 587 –596.
6. T. Klotz, W. Bloch, C. Volberg, U. Engelmann, K. Addicks, *Cancer*, 1998, **82**, 1897– 1903.
7. L. C. Jadeski, K. O. Hum, C. Chakraborty, P. K. Lala, *Int. J Cancer*., 2000, **86**, 30– 39.
8. L. C. Jadeski, P. K. Lala, *Am. J. Pathol*., 1999, **155**, 1381–1390.
9. G. R. Swaroop, P. A. Kelly, H. S. Bell, J. Shinoda, S. Yamaguchi, I. R. Whittle, *Br. J . Neurosurg*., 2000, **14**, 543–548.
10. B. Sanna, M. Debidda, G. Pintus, B. Tadolini, A. M. Posadino, F. Bennardini, G. Sava, C. Ventura, *Arch. Biochem. Biophys*., 2002, **403**, 209–218.
11. A. Vacca, M. Bruno, A. Boccarelli, M. Coluccia, D. Ribatti, A. Bergamo, S. Garbisa, L. Sartor, G. Sava, *Br. J. Cancer*., 2002, **86**, 993–998.
12. E. Tfouni, D. R. Truzzi, A. Tavares, A. J. Gomes, L. E. Figueiredo, D. W. Franco, *Nitric Oxide*, 2012, **26**, 38–53.
13. B. Serli, E. Zangrando, T. Gianferrara, L. Yellowlees, E. Alessio, *Coord. Chem. Rev*., 2003, **245**, 73–83.
14. L. Morbidelli, S. Donnini, S. Filipi, L. Messori, F. Piccioli, G. Sava, M. Ziche, *Br. J. Cancer*, 2003, **88**, 1484–1491.
15. C. G. Hartinger, M. A. Jakupec, S. Zorbas-Seifried, M. Groessl, A. Egger, W. Berger, H. Zorbas, P. J. Dyson, B. K. Keppler, *Chem. Biodiversity*, 2008, **5**, 2140–2155.
16. C. G. Hartinger, S. Zorbas-Seifried, M. A. Jakupec, B. H. Zorbas, B. K. Keppler, *J. Inorg. Biochem.*, 2006, **100**, 891–904.
17. A. K. Bytzek, K. Boeck, G. Hermann, S. Hann, B. K. Keppler, C. G. Hartinger G. Koellensperger, *Metallomics*, 2011, **3**, 1049–1055.

18. L. Morbidelli, S. Donnini, S. Filipi, L. Messori, F. Piccioli, G. Sava, M. Ziche, *Br. J. Cancer*., 2003, **88**, 1484–1491.

19. T. Storr, B. R. Cameron, R. A. Gossage, Y. Yee, R. T. Skerlj, M. C. Darkes, S. P. Fricker, G. J. Bridger, N. A. Davies, M. T. Wilson, K. P. Maresca, J. Zubieta, *Eur. J. Inorg. Chem*., 2005, 2685–2697.

20. M. Oszajca, E. Kulis, G. Stochel, M. Brindell, *New. J. Chem.*, 2014, **38**, 3386-3394.

21. B. Serli, E. Zangrando, E. Iengo, G. Mestroni, L. Yellowlees, E. Alessio, *Inorg. Chem*., 2002, **41**, 4033–4043.

22. B. R. Cameron, M. C. Darkes, H. Yee, M. Olsen, S. P. Fricker, R. T. Skerlj, G. J. Bridger, N. A. Davies, M. T. Wilson, D. J. Rose, J. Zubieta, *Inorg. Chem.*, 2003, **42**, 1868–1876.

23. R. Mosi, B. Seguin, B. Cameron, L. Amankwa, M. C. Darkes, S. P. Fricker, *Biochem. Biophys. Res. Commun.*, 2002, **292**, 519-529.

24. M. J. Clarke, *Coord. Chem. Rev*., 2002, **232**, 69–93.

25. T. Storr, B. R. Cameron, R. A. Gossage, H. Yee, R. T. Skerlj, M. C. Darkes, S. P. Fricker, G. J. Bridger, N. A. Davies, M. T. Wilson, K. P. Maresca, J. Zubieta, *Eur. J. Inorg. Chem*., 2005, **2005**, 2685–2697.

26. M. J. Frisch, G. W. Trucks, H. B. Schlegel, G. E. Scuseria, M. A. Robb, J. R. Cheeseman, G. Scalmani, V. Barone, B. Mennucci, G. A. Petersson, H. Nakatsuji, M. Caricato, X. Li, H. P. Hratchian, A. F. Izmaylov, J. Bloino, G. Zheng, J. L. Sonnenberg, M. Hada, M. Ehara, K. Toyota, R. Fukuda, J. Hasegawa, M. Ishida, T. Nakajima, Y. Honda, O. Kitao, H. Nakai, T. Vreven, J .A. Montgomery, J. E. Peralta, F .Ogliaro, M. Bearpark, J. J. Heyd, E. Brothers, K. N. Kudin, V. N. Staroverov, T. Keith, R. Kobayashi, J. Normand, K. Raghavachari, A. Rendell, J. C. Burant, S. S. Iyengar, J .Tomasi, M. Cossi, N. Rega, J. M. Millam, M. Klene, J. E. Knox, J. B. Cross, V. Bakken, C. Adamo, J. Jaramillo, R. Gomperts, R. E. Stratmann, O. Yazyev, A. J. Austin, R. Cammi, C. Pomelli, J. W. Ochterski, R. L. Martin, K. Morokuma, V. G. Zakrzewski, G. A. Voth, P. Salvador, J. J. Dannenberg, S. Dapprich, A. D. Daniels, O. Farkas, J. B. Foresman, J. V. Ortiz, J. Cioslowski, D. J. Fox, Gaussian 09 (Revision B.01), Gaussian Inc., Wallingford, CT, 2010.

27. C. Lee, W. Yang, R.G. Parr, *Phys Rev*., 1988, **37**, 785-789.

28. P. J. Hay, W. R. Wadt, *J. Chem. Phys.*, 1985, **82**, 270-284.

29. J. P. Perdew, K. Burke, Y. Wang, *Phys. Rev. B*, 1996, **54**, 16533-16539.

30. C. Gonzalez, H. B. Schlegel, *J. Chem. Phys.*, 1989, **90**, 2154-2161.

31. C. Gonzalez, H. B. Schlegel, *J. Phys. Chem.*, 1990, **94**, 5523-5527.

32. D. V. Deubel, J. K. C. Lau, *Chem. Commun.*, 2006, 2451-2453.

33. J. K. C. Lau, D. V. Deubel, *J. Chem. Theory Comput.*, 2006, **2**, 103.

34. V. Barone, M. Cossi, *J. Phys. Chem. A*, 1998, **102**, 1995-2001.

35. J. Chen, L. Chen, L. Siyan, K. Zheng, L. Ji, *J. Phys. Chem. B*, 2007, **111**, 7862-7869.

36. K. A.Connors, *In Chemical Kinetics-The Study of Reaction Rate in Solution*; Wiley: New York, 1990, pp 200.

37. E. Alessio, G. Balducci, A. Lutman, G. Mestroni, M. Calligaris, W. M. Attia, *Inorg. Chim. Acta*, 1993, **203**, 205-217.

38. B. R. Puri, L. R. Sharma, K. C. Kalia, *Principles of Inorganic Chemistry*, Vallabh Publications, 1966.

39. M. Bouma, B. Nuijen, M. T. Jansen, G. Sava, A. Flaibani, A. Bult, J. H. Beijnen, *Int. J. Pharm.*, 2002, **248**, 239-246.

40. M. Bouma, B. Nuijen, M. T. Jansen, G. Sava, F. Picotti, A. Flaibani, A. Bult, J. H. Beijnen, *J. Pharm. Biomed. Anal.*, 2002, **30**, 1287-1296.

41. V. S. Sharma, T. G. Traylor, R. Gardiner, H. Mizukami, *Biochemistry*, 1987, **26**, 3837-3843.